methods of synthesis such as using chemical synthesis procedures using strong oxidising agents to obtain Graphene oxide. In this method, GO is readily synthesized by the oxidation of the natural flake graphite powder. This procedure of GO synthesis is attractive due to its low cost, and widespread availability of graphene [52]. Three popular methods exist for the synthesis of GO viz., the Brodie method, Staudenmaier method and Hummers method and all involve the oxidation of graphite using strong acids and oxidants. The Brodie and Staudenmaier methods encompass the use of a combination of potassium chlorate ($KClO_3$) with nitric acid (HNO_3) to oxidise graphite [53]. These two methods, however, rely on a lengthy oxidation step which may take up to a week. Hummer's method is, thus, the most commonly preferred method. This method uses H_2SO_4 as the intercalant while the oxidising agents used are $NaNO_3$/$KMnO_4$. The oxidation step in this method is much shorter than for other methods and can be completed within 2 hours. One problem which has arisen from this method is the release of NO_x and ClO_2, which are toxic gases, into the environment and has led researchers to develop improved Hummers methods in which the production of these toxic gases are eliminated. These new methods were dubbed modified-Hummer's methods and their synthesis processes have proven to yield higher quality graphene sheets with distinct properties [54].

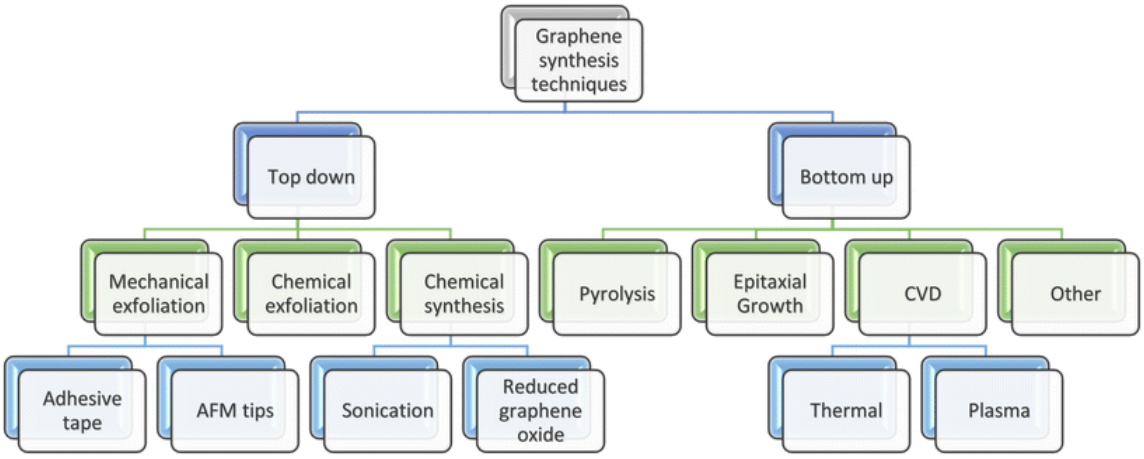

Figure 6: Synthesis methods of Graphene

Allahresani synthesized a Mn(II)Salen complex immobilized onto graphene oxide, which was modified by 3-chloropropyltrimethoxy silane. This synthesized material was used as a heterogeneous catalyst. The advantages of this catalyst is its enhanced properties due to the immobilisation of the graphene oxide material improving the surface area and thus enhancing the catalytic properties [55].

Saroja and Bhat described an easy pathway for the immobilisation of a cobalt-Schiff base complex onto graphene oxide using APTMS to functionalise the GO. The synthesized sample was characterised using various techniques such as FTIR, SEM, and TEM. From their experimentation, it was deduced that GO as a supporting material, was extremely advantageous as it possesses high surface area as well as thermal and chemical stability [56].

Graphene and reduced graphene oxide is appealing for electrochemistry, specifically for electrode modification as it facilitates a direct electron transfer process and improves the electron transfer efficiency [41] and has been used extensively in various voltammetric applications as a means to improve the sensitivity offering more desirable results.

Graphene oxide may also be immobilized onto ligands and metal complexes acting as a support while also providing these augmented properties.

Nanoscience in South Africa

In order for South Africa (SA) to progress from a resource-based economy towards a knowledge-based economy, it had to look for innovative solutions to provide promising contributions for economic progression. This has led SA to turn to Science and technological based strategies in coming up with a suitable 10-year plan to achieve its national goals, which includes enhancing economic growth, industrial competitiveness, as well as social and developmental aspirations. South Africa thus integrated a National Research and Development strategy in 2002 to help achieve these goals.

One of the widely sought-after areas of interest which were highlighted by the National Research and Development Strategy was Nanoscience and Nanotechnology (N&N) as it is believed that it may provide a meaningful contribution to the economy through promising scientific breakthroughs. Nanoscience may also have a positive impact on our economy through various productive collaborations with international countries and institutions as well as publications in the research communities. The transition toward a knowledge-based economy and away from a resource-based economy has the ability to promote advancement and support various key areas in South Africa such as health, water and energy.

The government has supported these objectives by establishing Nanotechnology innovation centres to produce cutting-edge research and extending research grants relating to nanoscience and nanotechnology research and by implementing an N&N master's research programme [57].

2.4 Nafion

Nafion is a conductive and water-insoluble perfluorinated polymer used to coat the electrode surface. Khanfar *et al.* investigated the enhancement of the detection sensitivity and selectivity through modification using nafion which provides a higher binding affinity towards the analyte and increases the electrical double layer's charge transfer-rate [58]. Modification of nafion onto electrode surfaces is commonly effected through dip-coated or electrodeposited methods [59]. The remarkable properties of nafion for electrode coating which may be useful for metal extraction includes the great mechanical and chemical stability that nafion coating provides while the exceptional ion-exchange properties enables rapid extraction via metal-ligand complexation [60].

2.5 Water Treatment (WT)

The water treatment industry has progressed rapidly due to the improvement of science and technology and has seen the industry reach new heights. Removal of heavy metal ions is one form of WT and various methods have been established for this specific purpose. These methods include advanced techniques such as chemical precipitation, ion-exchange, electrochemical removal [61], ultrafiltration and reverse-osmosis [62] which have been applied successfully to remove pollutants that are not able to be completely removed by conventional methods.

Chemical Precipitation (CP)

Zamboulis *et al.* described the conventional methods for treating metal containing effluent and its disadvantages [63]. The chemical precipitation method is one of the most widely used heavy metal removal methods in industry for inorganic effluent due to its

convenient operation. In the chemical precipitation method, water containing the heavy metals is treated using chemicals to increase the pH causing precipitation and promoting flocculation. The insoluble solid precipitate is then removed by sedimentation, dehydration and then must be disposed in expensive landfills. The main drawbacks of the chemical precipitation method is that the problem is only diverted from liquid to solid form and that the chemicals used are non-recyclable [64].

Ion-exchange (IE)

The ion-exchange technique along with many other techniques was researched by Gunatilake as an industrial water treatment process. The ion-exchange method is a cost-effective method in which soluble ions are attracted from the liquid to the solid phase. It's widely used in industry due its simple operation and low-cost materials and has been proven to effectively remove low concentrations of heavy metals. Cations and anions consisting of water-insoluble solid special ion exchangers, such as organic ion exchange resins, are used for the heavy metal ion removal from solution. These IE resins are able to absorb positively or negatively charged ions from an electrolyte solution while releasing equivalent amounts of same charged ions [65]. Zhang *et al.* synthesized a new type of adsorbent material, utilising reduced graphene oxide grafted by 4-sulfophenylazo groups, which was used to adsorb heavy metal ions via ion-exchange. The maximum adsorption capacities for Cu(II), Ni(II), Cr(II), Cd(II) and Pb(II) were found to be 59, 66, 191, 267 and 689 mg/g, respectively. Therefore an efficient water treatment method was established for the removal of these metal ions using the ion-exchange method [66].

Reverse Osmosis (RO)

Arezoo Azimi reviewed the reverse osmosis method of water treatment. The reverse osmosis process has found application in various industries such like desalination, food processing, biotechnology and pharmaceutics. It is a rudimentary separating technological treatment used for the removal of heavy metal ions. RO is characterised by a pressure-driven membrane process using a hydraulic operating pressure and a semi-permeable membrane which prohibits the flow of certain particles through it. The underlying principle of reverse osmosis includes the absorption of heavy metals onto the membrane surface once the polluted water passes through. Then diffusion occurs through the membrane due to the concentration gradient causing the water molecules to move down the gradient to the membrane's permeate side. Once the separation is completed, the feed side of the membrane will contain the concentrated heavy metal solution while the permeate side will contain the treated solution. The resulting pollutants must be treated according to certain standards. The efficiency of the separation is related to the solute properties such as size, charge exclusion and physico-chemical interactions between the solute, solvent and membrane [67].

Electrochemical Methods

Electrochemical methods as a means of water treatment have gained considerable attention in recent years as cost effective and convenient heavy metal removal technologies. The advantages of this type of method over others is that it does not require high temperatures or high pressures like other techniques and is still able to provide robust performance [68]. In this method, electricity is applied to remove the metal ion in its metallic form. The electrodeposition occurs at the electrode surface and does not

require any chemicals for its usage causing no un-wanted by-products. Since the electron is the main reagent of the reaction, the EC method is considered to be a clean, environmentally friendly technological method for the removal of heavy metals [64].

The electrode is important in this process and has attracted lots of interest from researchers for enhanced performance electrode surfaces to be achieved. Modification of these electrodes has been at the forefront of electrochemical wastewater treatment research and nanoscience has been earmarked to provide desirable electrode.

2.6 Novelty of this work

As previously discussed, several methods of water treatment exist, each with its own benefits and drawbacks. The electrochemical method was selected for the removal of heavy metal ions in that it is cheaper, environmentally friendly and does not produce any unwanted by-products. The electrode is of utmost importance in this process, and its ability to be modified has been the core focus of this research. The electrode of interest was the glassy carbon electrode due its remarkable electrical and mechanical properties and the ability for modification. The electrode surface was modified with Salen and salen type ligands by way of the formation of a modification ink. The salen-type ligand was also immobilised onto graphene, via functional groups, affording even greater sensitivity, selectivity and electrical conductivity. The ligands were also modified with nafion and coated onto the GCE and their extraction ability as well as detection abilities were researched. Salen and salen-type ligands were chosen as they are easily synthesized and form complexes with most metals via the chelating effect.

In this work, the square-wave voltammetry electrochemical method was used for experimentation owing to its high sensitivity to surface-confined electrode reactions. The

voltammetric experiments were run from more positive to more negative potentials thereby inducing oxidation of the analytes (the oxidative properties were investigated due to the reduction peaks being much smaller as seen in the results section). The salen modified electrodes were used to allow removal of the heavy metals via complexation on the glassy carbon electrode double layer. Salen-type modified electrodes were explored to determine their chelation with the heavy metal ions. This was the ex-situ method of experimentation. Another method, called the in-situ method, was investigated whereby the heavy metal ions were added to the voltammetric cell along with the ligand solution and the contents of the cell were stirred allowing for complexation to proceed. Subsequently, the resulting metal complex was analysed. The metal complexes of interest were all synthesized prior to experimentation in order to compare with the results of the in-situ and ex-situ methods. Extraction studies were conducted to investigate the extraction performance of each extraction method.

CHAPTER 3: EXPERIMENTAL METHODOLOGY

3.1 Introduction

This chapter entails the materials, instrumentation, experimental procedures and synthesis protocols. It also describes the preparation of the electrodes as well as the electrode modification procedures. The various characterization techniques and their specificity for this work is described with emphasis placed on the electroanalytical techniques.

3.2 Materials

All reagents used in this work were analytical reagent grade and used without further purification. The table below indicates the reagents and their origin.

Table 2: Table of reagents and their source

Reagents	**Supplier**
Meta atomic absorption standard solution 1000 mg/L	Fluka
Salen	Aldrich
Salicylaldehyde	Aldrich
Diethylenetriamine	Sigma-Aldrich
1,3-Diamino-2-propanol	Sigma-Aldrich
Cobalt chloride	B & M Scientific
Nickel chloride	Fluka
Copper nitrate	Saarchem
Sodium acetate	Sigma-Aldrich
Acetic acid	Sigma-Aldrich
Sodium phosphate dibasic stock	Sigma
Sodium phosphate monobasic stock	Sigma-Aldrich
Nafion (5 wt%)	Aldrich
Glacial acetic acid	Saarchem
Hydrochloric acid	Sigma-Aldrich
Dimethylformamide	Kimix
Absolute ethanol	Kimix

3.3 Characterisation

The ligands, chelating complexes and as- synthesized graphene were characterised using various techniques such as: FTIR, GC-MS and NMR Spectroscopy. These techniques are briefly discussed and summarized.

Fourier Transform Infrared Spectroscopy (FTIR)

FTIR is a vibrational spectroscopic technique used to provide the molecular fingerprint of a sample by analysing its chemical composition information [69]. In FTIR, information is obtained by how much light (i.e. infrared) a sample absorbs at a certain wavelength owing to the fact that molecular bonds absorb infrared light at frequencies characteristic to their vibrations [70]. FTIR analysis is dependent on the atoms involved in the bonds and the strength of the intermolecular interactions rendering unique spectrums for each molecule. IR spectroscopy is a simple, low-cost technique which requires simple sample preparation for it usage [71].

Nuclear Magnetic Resonance Spectroscopy (NMR)

Nuclear Magnetic Resonance (NMR) spectroscopy is a powerful and robust analytical method that exploits the magnetic properties of certain nuclei such as 1H, 13C, 21P and 19F. NMR can be applied to liquid and/or solid materials and it is mainly used to measure the concentration of various molecules in a sample, study the interaction between them, and elucidate the structure of organic compounds and biomolecules. [75]. In NMR spectroscopy, individual atoms are studied yielding information about the relationship between all Hs and Cs and selected heteroatoms of a molecule [76] as well as contributing structural information [77]. Two methods of NMR Spectroscopy exist, ^{1}H NMR and ^{13}C

NMR, both operating under the same underlying principles with the only difference being their gyromagnetic ratio and resonance frequencies [78] with the one providing information on the molecules Hydrogen bonds and the other the Carbon bonds.

Gas chromatography/ Mass Spectrometry (GC-MS)

GC-MS is an advanced separation chromatographic system which is robust and provides highly reproducible results for compound identification [79]. Characterization of compounds are usually achieved through sufficient information obtained by a molecular ion (equivalent to molecular weight) and pattern of fragment ions [80].

3.4 Electrochemical Characterisation

Electrochemistry

Electrochemistry is a handy and powerful method of probing electron transfers within reactions by relating the flow of electrons to chemical changes observed [81]. Therefore, electrochemistry can give researchers and analytical scientists information on reaction mechanisms, electron kinetics, electron thermodynamics and ion transfer processes [82].

History of electrochemistry and voltammetry

Electrochemistry forms part of many branches of chemistry and is well integrated in the disciplines of physical, organic, inorganic and analytical chemistry. Although electrochemistry forms a part of these main branches of chemistry, modern electrochemistry was founded long before these other sciences ever existed. It dealt with the electron a whole century before the electron was discovered at the dawn of the 20th century. "Modern electrochemistry" was started in the 18th and 19th century by Alessandro

Volta and other scientists. This modern electrochemistry allowed scientists of the time to isolate and discover about ten chemical elements and various applicable products in a short time span. Thus, electrochemistry provided support and assistance for the progression of other sciences.

Although Volta was credited as the founder of electrochemistry, due to his invention of the first D.C power source which was able to split water into oxygen and hydrogen, Luis Galvani was initially the first to discover electricity. Galvani's discovery came accidently as he brought two metals into contact, generating electricity which made dead body parts move (for e.g. The frogs leg) [83].

From electrochemistry, a further branch was developed called Voltammetry. The term "Voltammetry" originates from the root word, "Voltam-" which refers to potential (volt) and current (am) [84]. In 1922, the Czech chemist Jaroslav Heyrovsky discovered voltammetry from polarography, which is a class of voltammetry incorporating a hanging mercury drop electrode as the working electrode, earning him the 1959 Nobel Prize in chemistry. However, these early voltammetric methods encountered numerous difficulties, preventing them for commercial routine analysis application. In the 1960's and 1970's, major advances in all aspects of voltammetry such as theory, methodology and instrumentation were made leading to enhanced sensitivity. These advances coupled with the emergence of relatively inexpensive amplifiers accelerated the commercialisation of low-costing voltammetric instrumentation [85].

Basics of voltammetry

In the voltammetry method of electroanalysis, a chemical signal (either concentration or amount of analyte) is converted into a physical signal (potential or current) which is then

transformed into an appropriate electrical signal which is processed by the electronic instrument and displayed as a readable signal for the operator to understand [86]. The excitation of the sample occurs simply by applying a potential (V) to the electrode. The current (i) is thus monitored as it flows through the electrochemical cell over a certain time (t). All voltammetric techniques can, hence, be described as some function of *E* (potential), *i* (current) and *t* (time).

The analytical advantages of voltammetric techniques include excellent sensitivity with a wide concentration range for both organic and inorganic species, a broad temperature range, various useful solvents and electrolytes, simultaneous multi-element analysis, rapid analysis times, able to determine kinetic and mechanistic parameters and the ability to reasonably estimate unknown parameters [85]. Further advantages of voltammetric techniques are characterised by the instrument simplicity, moderate cost, portability and low sample consumption [87].

Voltammetry theory

The transfer of electrons is associated with the electrode process taking place across the electrode/solution interface (also known as the Electrical Double Layer). The double layer consists of several layers: an inner layer, also called the Helmholtz or Stern layer, closest to electrode which contains the solvent molecules and sometimes other species (ions or molecules) which have been specifically adsorbed. The diffuse layer is the layer between the adsorbed layer and the bulk of the solution and contains ions which are said to be non-specifically adsorbed. The structure of this electrical double layer influences the electrode processes rate [88].

The electrode process causes the reduction or oxidation of the electroactive species A according to the following general reversible reaction:

$$Ox\ (A) + ne \leftrightarrows Red\ (B)$$

Upon oxidation, species A is consumed, and B is produced at the electrode surface. The mass transport of A to the electrode surface and B from the surface occurs through three possible classifications [89]:

- Migration: dependent on the potential drop in the solution
- Diffusion: due to the concentration gradient at the electrode surface
- Convection: originating in flowing systems

The relationship between the applied potential and the surface concentrations of oxidation and reduction is described by two well-known laws; the Nernst equation and the Butler-Volmer equation. Eq. 1 is a typical redox reaction and its equilibrium state is governed by the Nernst equation. The Nernst equation stays true for thermodynamically reversible electrochemical reactions because as the potential is varied, the equilibrium is re-established. The Nernst equation is given below:

$$E = E^o + \frac{RT}{nF} \ln \frac{c(Ox)_{x=0}}{c(Red)_{x=0}} \qquad \textbf{Equation 1}$$

Where,

E = cell potential

E^o = standard redox potential for the ox/red couple

R = Gas constant (8.314 J K^{-1} mol^{-1})

T = Absolute temperature (K)

n = number of electrons transferred

F = Faradays constant (9.648 x 10^4 C mol^{-1})

At room temperature (25°C), $\frac{RT}{F}$ may be treated as a constant and replaced by 25.693 mV for cells.

It is often useful to know the relation that links current, potential and concentration. The rate of a reaction is controlled only by the rate of the electrical charge transfer process and is given by the Butler-Volmer equation, which is an activation-controlled reaction [21]. This equation allows for the estimation of the standard rate constant of electron transfer *k*, and is given by:

$$\frac{i}{nFA} = k^0\{{c_{ox}}^0 \exp[-\alpha\theta] - {c_{red}}^0 \exp[(1-\alpha)\theta]\} \qquad \textbf{Equation 2}$$

Where,

θ = nF(E-E^0)/RT

k^0 = heterogeneous rate constant

α = transfer coefficient

A = electrode area

Common voltammetric techniques

Various voltammetric techniques have been adapted in recent times for a range of applications such as cyclic voltammetry (CV), differential pulse voltammetry (DPV), square-wave voltammetry (SQW) and linear sweep voltammetry (LSV). These methods give both quantitative and qualitative data with magnificent precision ($< 1\%$), enhanced sensitivity and a wide linear dynamic range [90]. Cyclic voltammetry and Square-wave Voltammetry are discussed as they are specific techniques related to this work.

Cyclic Voltammetry (CV)

Cyclic Voltammetry is the most conventional electroanalytical technique utilised for the acquisition of qualitative information relating to electrochemical reactions. CV provides a swift location of both the oxidation and reduction potentials of the electroactive species reaction which takes place at the working electrode.

In CV, the voltage is swept between two values at a fixed rate and starts from an initial potential until it reaches a set final potential value. The sweep is then reversed until the voltage reaches the initial potential value [91]. If the scan begins at a negative potential, the forward scan will be oxidation and vice-versa. The peak current, peak potential and characteristic shapes of the voltammograms essentially fingerprint the individual electrochemical properties of the redox system illustrating information such as the type of electrode reaction, number of electrons exchanged and as well as adsorption reactions [88, 92]. The magnitude of the current and the current are directly proportional to one another (Fig. 7) [84].

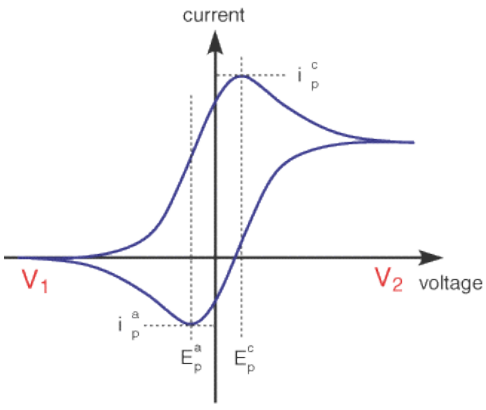

Figure 7: A typical cyclic voltammogram recorded for a reversible single electrode transfer reaction for a solution containing only a single EC reactant

Square-Wave Voltammetry (SQW)

Square-wave voltammetry is one of the most advanced of the four major voltammetric techniques along-side CV, DPV and LSV. It has achieved widespread application over the last decade owing to the commercialisation of the voltammetric instrument as an electroanalytical tool. Other factors leading to SQW application include its theory being well-developed and because of its high sensitivity to surface-confined electrode reactions [93]. This high sensitivity is achieved by replacing the continuous potential ramp of the CV technique with a staircase potential combined with small potential pulses, equal in height but opposite directed potential [94], thereby diminishing the contribution of the charging current. The current is measured at the end of each potential pulse diminishing the charging current drastically, thus enhancing the sensitivity and improving upon the voltammetric data achieved. The main parameters of the SQW method include the height of a single pulse, called the square-wave amplitude (Esw), the scan increment (ΔE) and the square-wave frequency (f), which is the duration of the potential pulse (Fig. 8) [95].

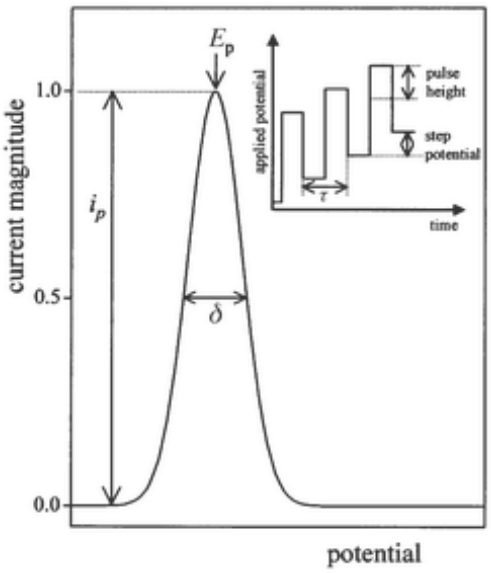

Figure 8: A typical Square-wave voltammogram including the potential cycle

The peak-like shape of the SQW component is advantageous as it provides measurable parameters such as peak height and peak position improving the techniques resolution. Since the overall shape of the SQW resembles the forward and reverse components of CV, mechanistic information is obtainable from the SQW method [95].

Square-wave voltammetry has been extensively used for the analysis of heavy metal ions due its advantageous properties. However, many other instruments have similar, if not better, properties so due diligence must be done before selecting the instrumentation for analysis. Other analytical methods such as Inductively coupled plasma spectroscopy (ICP) and Graphite furnace atomic absorption spectroscopy (GFAAS) have been used for heavy metal analysis. These methods hold some superiority in that they have a higher sensitivity, yet they are quite expensive and require highly skilled personal to operate them.

Voltammetric Instrumentation

The voltammetric electrochemical cell (Fig. 9) and equipment typically consists of two or three electrodes (depending on the electrode system), electrolyte solution, sample of interest and the equipment represents the electrical instrument, or potentiostat, whereby the voltage and other parameters are controlled. The potentiostat contains three electric terminals through which the electrodes are connected [96]. These electrodes are the working electrode (WE), the counter electrode (CE) and the reference electrode (RE). The applied potential from the potentiostat is measured against the reference electrode; the counter electrode allows the current to pass by closing the electrical circuit. The REs mainly used are Ag/AgCl (3 M KCl) and the saturated calomel electrode while commonly

used CEs are platinum wire, Au or even graphite. The electrochemical cell in which the sample and electrolyte is contained may come in various shapes, sizes and materials depending upon the amount of sample and technique used. The most important of the electrodes is the working electrode and thus a large emphasis is placed on selecting the appropriate one [97].

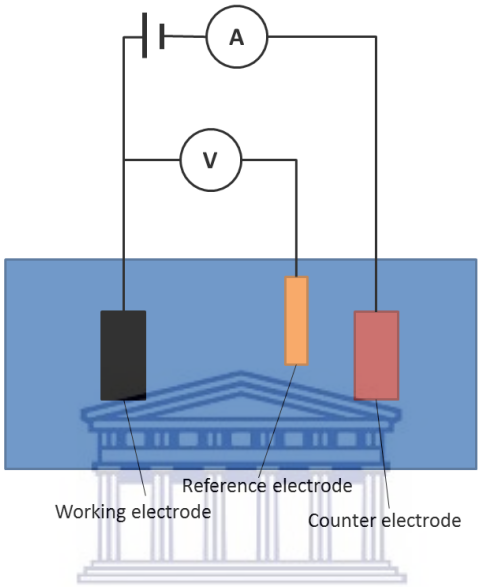

Figure 9: Schematic representation of a three-electrode electrochemical system consisting of a working, reference and a counter electrode

3.5 Instrumentation

Electro-analytical studies were performed using the 797 VA Computrace Potentiostat (Metrohm) connected to a computer for recorded data to be measured and evaluated (Fig. 10). The three-electrode system comprises a GCE/PGE, Ag/AgCl/KCl and a platinum wire as the working electrodes, reference electrode and counter electrode, respectively. The glassy carbon electrode was obtained from Basi and the Pencil graphite electrodes were HB, Pentel graphite rods. The measuring techniques performed were the square-wave voltammetry and cyclic voltammetry techniques. SQW was also used as a water

treatment method to remove metal ions via in-situ and ex-situ methods. All experiments were performed in an electrochemical cell at ambient temperature.

Figure 10: Computrace Potentiostat instrument 797 VA

FTIR results were recorded using a Perkin Elmer FTIR Spectrometer to provide information on the structures of the analytes of interest. IR spectra of the sample was recorded either as a neat using ATR (Attenuated total reflectance) (Fig. 11) or the sample was diluted with the IR-inactive KBr

Figure 11: Image of FTIR Spectrometer

NMR experiments were performed using a Bruker 400 MHz NMR spectrometer to provide information on the molecular structure of the samples.

3.6 Synthesis Protocols

Schiff base ligands

Two Schiff base ligands were prepared by reacting primary amines with carbonyl precursors of interest to achieve the intended salen-type ligands. The reactants were dissolved in ethanol in a 1:2 molar ratio (amine: carbonyl precursor) and kept in a round-bottom flask which was subjected to reflux for 4 hours. Thereafter, the product was collected, recrystallized and dried.

Salen ligand

For the synthesis of Salen (Fig. 13); ethylenediamine and salicylaldehyde in a 1:2 molar ratio is reacted under reflux for 4 hours as described in the protocol above.

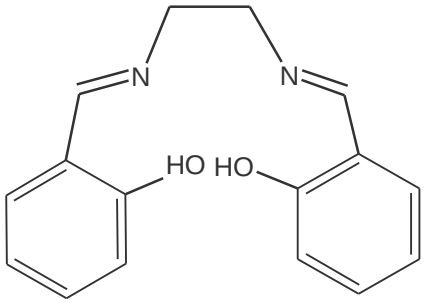

Figure 12: Chemical structure of Salen ligand (MW= 268.31 g/mol)

Sal-DAP

1,3-bis(salicylideneamino)-2-propanol (Fig. 14) was synthesised by reacting a 2:1 molar ratio of salicylaldehyde to 1,3-diamino-2-propanol under reflux as described above.

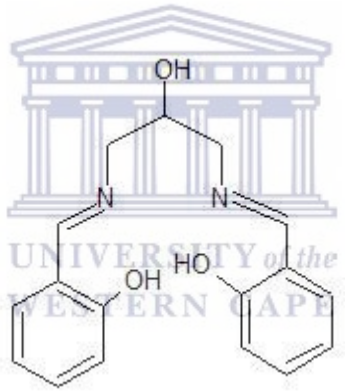

Figure 13: Chemical structure of 1,3-bis(salicylideneamino)-2-propanol (MW= 298.33 g/mol)

Metal Complexes

Metal complexes were produced by reaction of the ligand with the specific metal ion (nickel, copper and cobalt) in 1:1 molar ratio under reflux. The ligand was dissolved in ethanol followed by the addition of the metal ion (nickel, copper and cobalt) and the reaction was heated under reflux for 3 hours. The reaction mixture was left overnight.

The complex was collected by filtration, washed with ethanol and distilled water and left to dry.

Stock Solutions

The stock metal ion solutions were prepared by diluting 1,000 mg L^{-1}, atomic adsorption standard solutions in nitric acid (2%).

Buffer/Acid Solutions

A 0.1 M Acetate buffer (pH=4.6) was prepared by mixing suitable amounts of sodium acetate salt with acetic acid in ultrapure water.

0.1 M Phosphate buffer (pH=7.2) was prepared by adding appropriate amounts of 0.1 M sodium phosphate monobasic solution to 0.1 M sodium phosphate dibasic solution until the desired pH of 7.2 was achieved.

Ammonia/ammonium chloride, NH_3–NH_4Cl, buffer solution (0.1 M and 1 M, pH 9.4) was prepared by mixing ammonium chloride and ammonia followed by dilution with ultrapure distilled water.

Glacial Acetic Acid

For the voltammetric experiments, a single drop of glacial acetic acid was added to the electrochemical cell containing phosphate buffer.

Graphene Oxide (GO)

Graphene oxide was synthesized according to the modified Hummers method [98].

Approximately, 1g of graphite powder and 1 g of $NaNO_3$ were placed in a 500 ml round bottom flask. 70ml of H_2SO_4 was added to the round bottom flask (containing $NaNO_3$ and graphite) and magnetically stirred for 15 minutes in an ice bath. The temperature was kept below 5 ºC. Thereafter 5g of $KMnO_4$ was slowly added over a period of one hour to maintain a temperature below 5 ºC. Once all the $KMnO_4$ was added, the solution was stirred for an additional hour. The colour of the solution changed from grey to dark green. Hereafter, 46 ml of deionized (DI) water was gradually added to the solution, controlling the temperature to not exceed 90 ºC. Upon the addition of DI water, the colour of the solution changed from dark green to dark brown. The solution was left to stir for another 30 minutes. Subsequently, 5.5 ml of oxidizing agent H_2O_2 was added and the remaining addition of 140 ml of DI water. The colour of the solution changed, once more, from a dark brown solution to a yellow, brown (mustard) colour. Once all the additions of solvents and reagents were completed, the reaction was left to stir for an additional hour to maintain a homogeneous suspension. The prepared GO was filtered and washed through centrifugation with 30% HCl solution.

Nafion-Ligand Modifying Ink

The Nafion-ligand ink was prepared by adding 1 x 10^{-2} M ligand (0.03 g for Salen) to 5 mL of 1 wt% nafion solution and was sonicated for 20 minutes.

3.7 Working Electrode

The working electrode used for the experimentation was the glassy carbon electrode (BASi) (Fig. 16).

Figure 14: Glassy carbon electrode

Electrode Preparation

The glassy carbon electrode required meticulous and thorough cleaning to obtain a "new electrode" after each run without damaging the electrodes. This was achieved by soft polishing the electrode with 1, 0.3 and 0.05 micrometer alumina for a few minutes and was rinsed with ethanol, ultrapure water and allowed to dry.

Electrode Modification

Drop-cast method

The GCE was modified by drop-casting 2 μL of a modified ink on the electrode surface and allowed to dry. The modification process had to be meticulous ensuring reproducible results.

Electrochemical reduction

GCE surfaces were modified with graphene oxide using electrochemical methods. The graphene oxide was reduced on the electrode by applying a deposition potential of -0.7 V for 120 s using cyclic voltammetry. The sweep conditions were set to a starting potential of -1.5 V, first vertex potential of 0.3 V and a second vertex potential of -1.5 V. the voltage

step and sweep rate was 0.005 V and 0.1 V/s, respectively. The number of sweeps was set to record 5 sweeps. The electrode was rinsed with ultrapure water to remove non-reduced graphene oxide and then allowed to dry.

3.8 Experimental Procedure

Cleaning of the voltammetric cell

To avoid contamination, the electrochemical cell and electrode were cleaned by rinsing with ethanol, water and the electrode was polished with alumina powder of 0.05 micron respectively, on a wet polishing cloth by pressing the electrode softly against the polishing surface. A SQW voltammetric was performed in 3 M HCl for 30 seconds to remove any other impurities and finally washing the whole system and cell with ultra-pure water and then allowing it to dry.

Square-wave voltammetry procedure

The electrode was inserted into the cell containing 10 mL of the buffer solution. The cell was purged with nitrogen gas for 300s before each run. The potentiostat was set to apply a potential from negative to positive causing oxidation of the sample. The parameters which were kept constant throughout were set as follows: Voltage step (V) = 0.004 V, Amplitude (V) = 0.02 V, Frequency (Hz) = 50 Hz) and Sweep rate (V/s) = 0.198 V/s. For oxidative voltammetric scans, the SQW experiments were run from more negative to more positive potentials (-1.5 V to 1.5 V).

Metal complex analysis

SQW analysis was performed to determine the peaks of metal complexes. Two methods of mixing were used to deposit a metal film which is capable of detecting selected heavy metal ions and yield admirable detection limits.

In-situ mixing method (IM)

The in-situ method involved the mixing of solutions of ligand and metal ion, which were added to the buffer, in the electrochemical cell. The cell contents were stirred for 600-900s to allow complexation to occur. Square-wave voltammetry was used for the analysis by varying the working electrodes being used.

Ex-situ mixing method (EM)

In the ex-situ method, a glassy carbon electrode was selected as the working electrode due to its ease of modification via the drop-casting method. The modification ink was drop-casted onto the GCE and allowed to dry. The modified electrode was then immersed in the electrochemical cell containing suitable amounts of the specific metal ion. The system was purged for 300 s with N_2 gas and a deposition time of 600s was selected to ensure that complexation took place at the electric double layer of the GCE.

Extraction of metal ions studies

Calibration curve

A calibration curve of concentration *versus* current was conducted to show the relationship between the metal concentration and the complex peak formation through the current detected. It was assumed that the complex formation took place on the

electrode surface via complexation between the metal ion and ligand in a 1:1 molar ratio. The studied concentrations were in the range of 100 ppb to 30 ppm.

Removal efficiency

Removal efficiency studies were also performed to show the effect of time on complex formation [99].

$$\text{Percentage removal (\%)} = \frac{C_i - C_{obs}}{C_i} * \mathbf{100} \qquad \textbf{Equation 3}$$

Where,

C_i = initial metal concentration

C_{obs} = observed metal concentration

Effect of buffer solution

The effect of various buffer solutions on the extraction ability of the ex-situ method was investigated to determine the best buffer to provide the optimum results. The buffers used are acetate buffer, ammonia-ammonium chloride buffer and phosphate buffer.

Reusability

The reusability of the modified electrode for heavy metal extraction was examined by extracting the heavy metals from a buffer solution containing metal ions and then stripping the metals ion off in a clean buffer solution. The electrode was then immersed once more into the metal containing buffer solution and the ex-situ method was applied to determine the reusability of the modified electrode.

CHAPTER 4: RESULTS AND DISCUSSION

4 Introduction

This chapter reports on the synthesis and characterisation of the Salen ligand and its metal complexes. The electrochemical studies screened the removal and detection of heavy metal ions using Salen ligand as a chelating agent via different electrochemical methods. The extraction ability in various buffer solutions via ex-situ and in-situ methods are reported in this chapter using cobalt and nickel Salen complexes. Calibration curves are included to investigate the effect of the concentration of the metal ions on complexation. The removal efficiency for both methods is examined as well as the reusability of the modified electrode.

4.1 Fourier-Transform Infrared Spectroscopy (FTIR)

FT-IR analysis was performed in order to obtain information on the functional groups of the samples. The samples were prepared by mixing small amounts of the compound with KBr powder. The mixture was pressed as a pellet to be analysed by the FT-IR instrument. The infrared spectral bands of the ligand and its copper complexes are are shown in Figs. 15 -18. The FTIR spectrum of the free ligand exhibits the characteristic bands at ~ 3056 and 1634 cm^{-1} corresponding to ν (OH) and ν (C=N) of the azomethine group, respectively [3]. However, the FTIR spectra of complexes showed ν (C=N) band around 1624 cm^{-1} compared with free ligand 1634 cm^{-1}. The lowering of ν (C=N) indicated that the azomethine nitrogen atom coordinated to the metal ions. The disappearance of ν OH band and appearance of two new additional bands at ~ 625 and 470 cm^{-1} for ν (M-O) and

ν (M-N) confirms the deprotonation of the -OH group and coordination of metal ions with the phenolate oxygen atom.

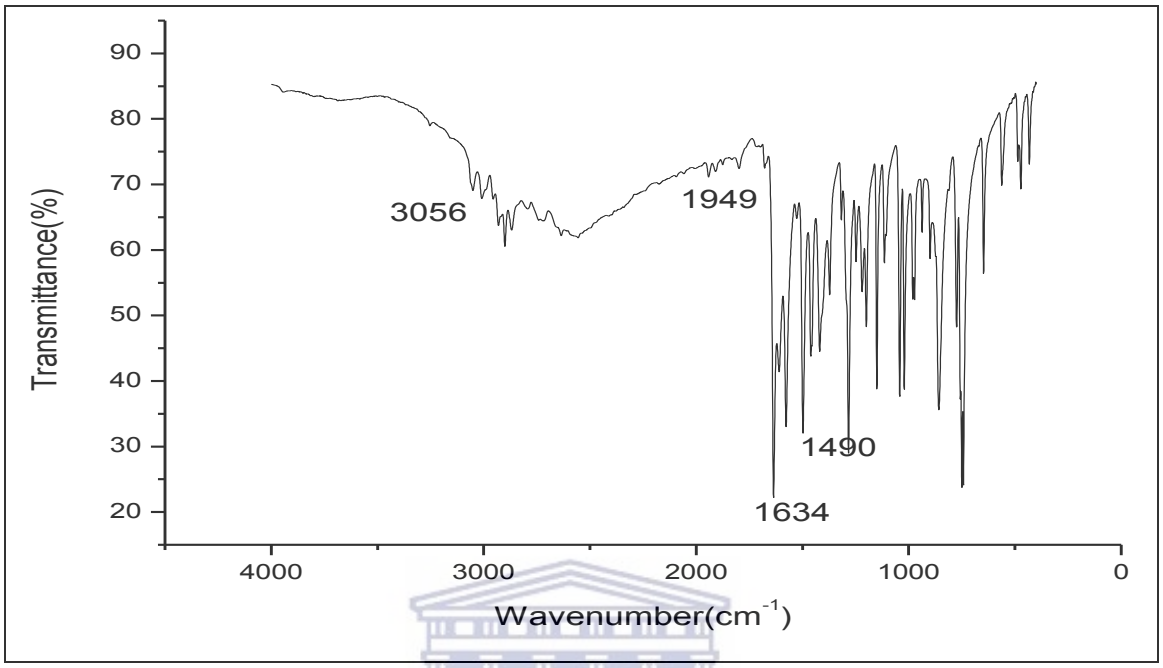

Figure 15: FTIR spectrum of Salen ligand

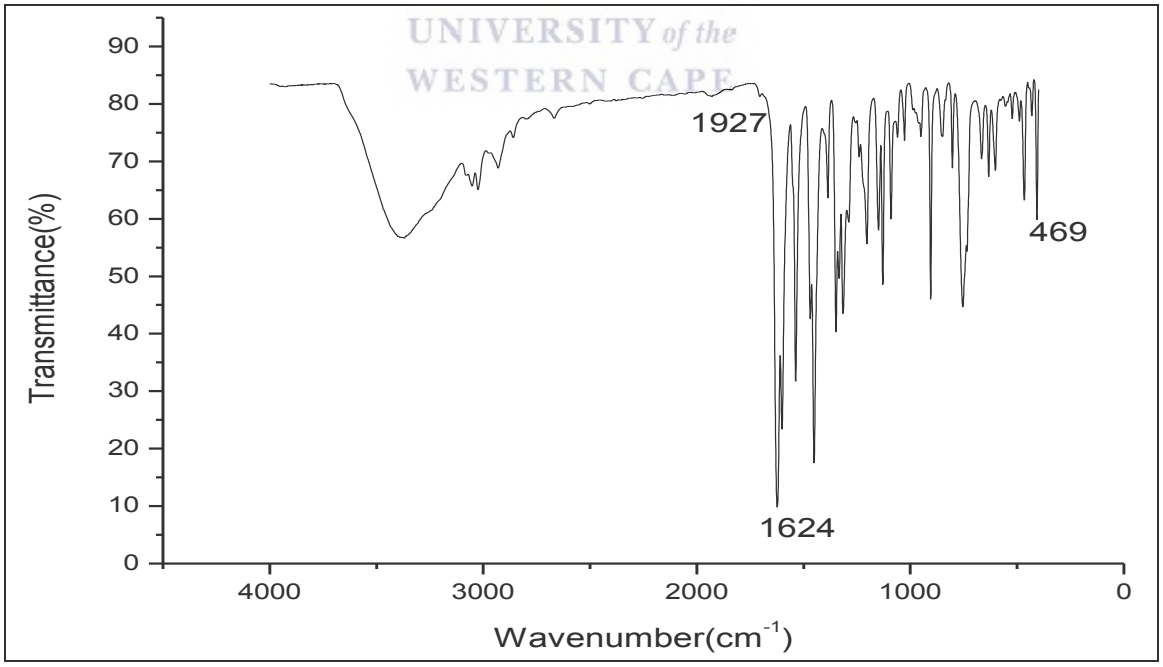

Figure 16: FTIR spectrum of nickel-Salen complex

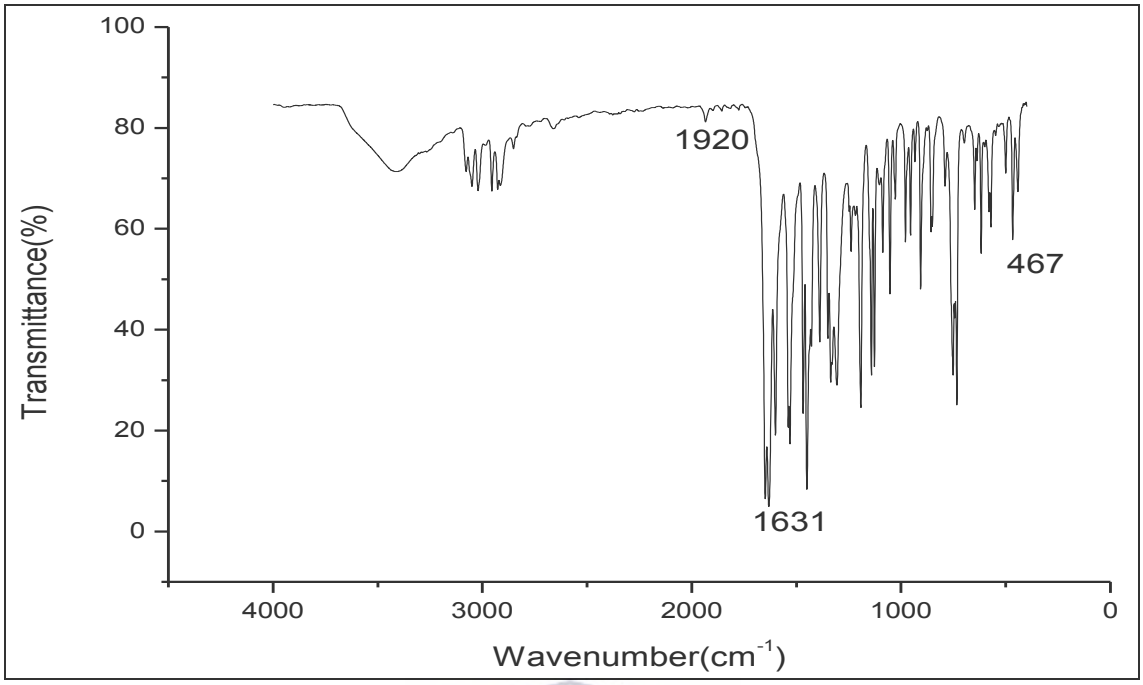

Figure 17: FTIR spectrum of copper-Salen complex

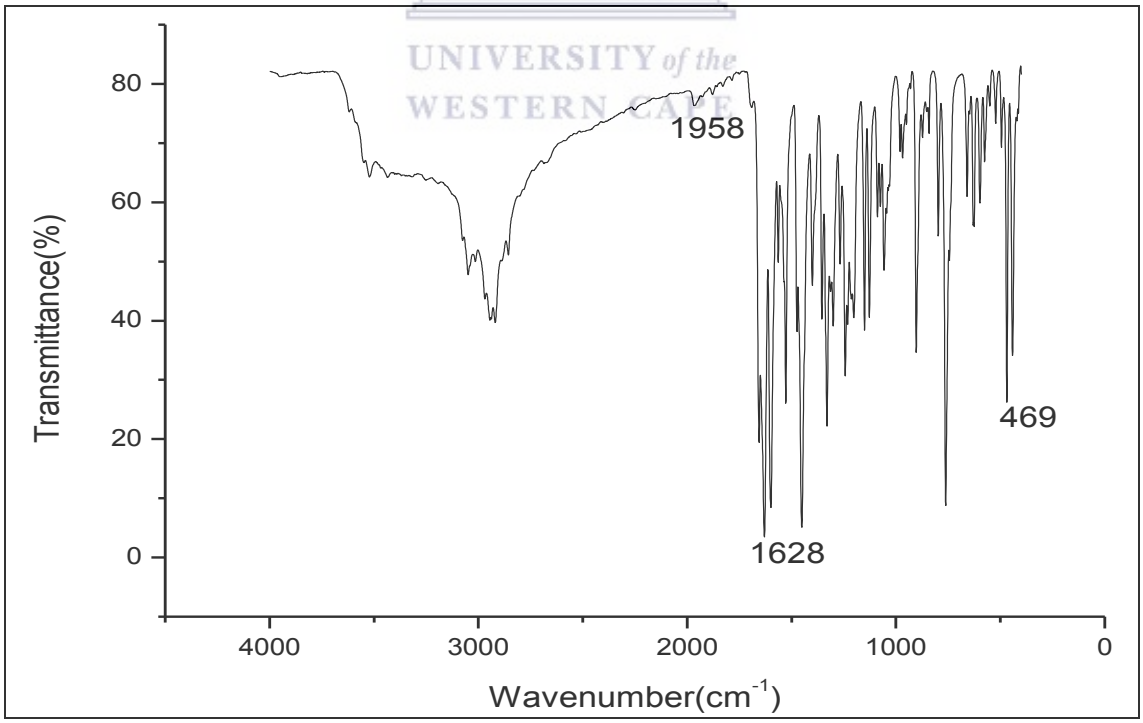

Figure 18: FTIR spectrum of cobalt-Salen complex

4.2 GC-MS

The Salen ligand was further characterized using GC-MS and the molecular ion and pattern of fragment ions are shown in Figure 19. The molecular ion (m/z) 268.2 [M^+] confirmed the ligand synthesis.

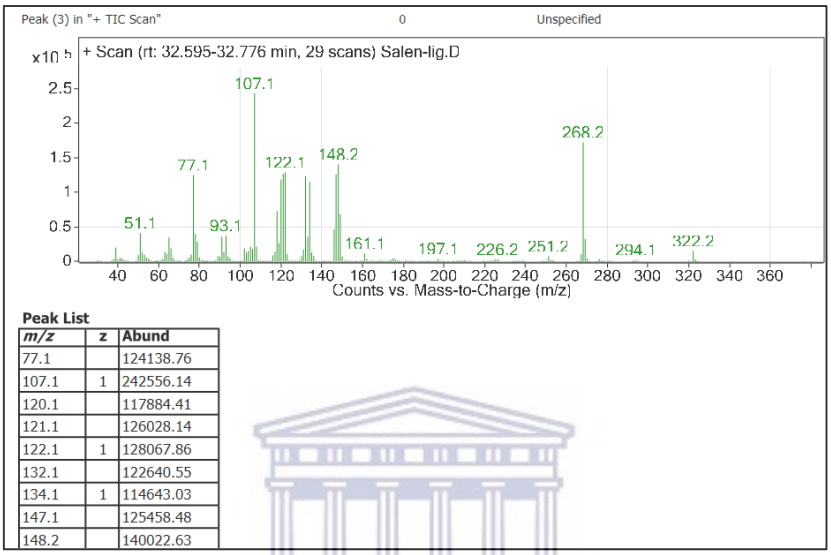

Peak List

m/z	z	Abund
77.1		124138.76
107.1	1	242556.14
120.1		117884.41
121.1		126028.14
122.1	1	128067.86
132.1		122640.55
134.1	1	114643.03
147.1		125458.48
148.2		140022.63

Figure 19: GC-MS chromatogram of Salen ligand

4.3 Electrochemical characterisation

The ligand (L) and copper(II) complexes were subjected to cyclic voltammetric studies to examine their electrochemical behaviour. A glassy carbon electrode was used as working electrode, platinum wire as auxiliary electrode and Ag/AgCl as reference electrode. The electrochemical studies were conducted in aqueous solution where the ligands and complexes concentrations were (1 x 10^{-4} M). Phosphate buffer solution (0.1 M) was used as supporting electrolyte. Measurements were made over a potential range between -1.5 to +1.5 V with a scan rate of 0.1 V/s

Electrochemical studies of Salen ligand

SQW of Salen Solution and Naf-Sal GCE

The Salen ligand solution and Salen-coated GCE electrode were electrochemically investigated to determine the Salen oxidation peak. This information provides a platform for further electrochemical investigations in order to compare the Salen ligand oxidation peak after complexing with various metal ions. To achieve that, a 2.5 x 10^{-4} M solution of Salen was added to the electrochemical cell and stirred for 300 s. The SQW was run from -1.5 to 1.5 V at a deposition time of 120 s. While Naf-Sal@GCE was modified by drop-casting 2 µL of the Naf-Sal ink onto the electrode surface and immersing it into the electrochemical cell containing the buffer solution to run SQW (Fig. 20). The oxidation peaks with shoulders were observed at 850 mV and 970 mV for the salen solution and Naf-Sal@ GCE, respectively. The oxidation peak is attributed to the oxidation of the imine bond (-C=N) of the ligand [5] which was shifted to a positive value in Naf-Sal@GCE indicating that this bond is harder to oxidize since electrons are not easily lost.

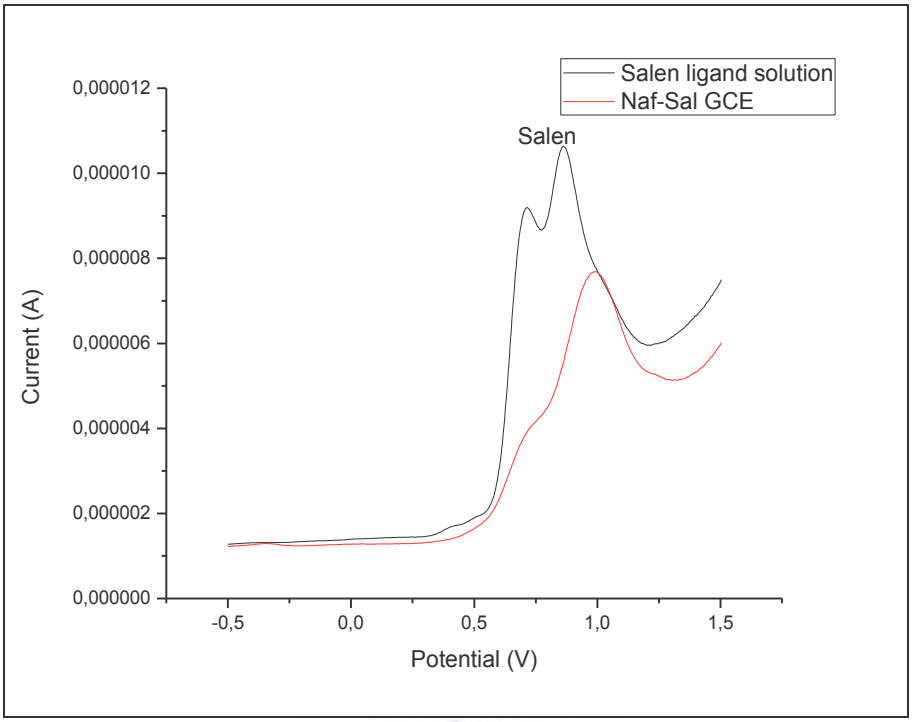

Figure 20: SQW voltammogram of Salen ligand and Naf-Sal@ GCE

SQW of Salen ligand and Cobalt metal ion

The electrochemical behaviour of the cobalt metal ion was examined by testing a 2.5 x 10^{-4} M solution thereof via an oxidation scan run from -1.5 to 1.5 V. At -1.5 V reduction takes place at the electrode surface which in turn causes the reduction of Co(II) to Co(I) until the reduction stops and oxidation proceeds. Thus, Co(I) is oxidised to Co(II) and Co(III) at specific potentials. Figure 21 exhibits a unique SQW oxidation voltammogram with three oxidation states for (Co). Two oxidation peaks are observed at -500 mV and 1.3 V attributed to the oxidation of Co(I) to Co(II) and Co(II) to Co(III), respectively.

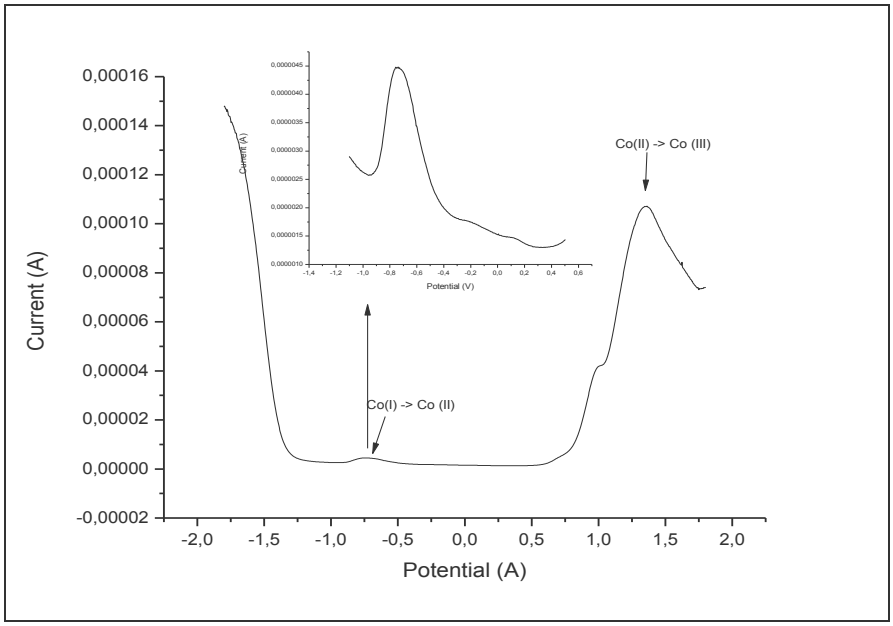

Figure 21: SQW oxidation scan of Co ion at bare GCE with expanded region (inset)

The oxidation scan of cobalt-Salen complex (2.5 x 10^{-4} M) illustrates oxidation peaks for the cobalt ion at -500 mV and 1.3 V and the Salen peak at 900 mV with a shoulder. The cobalt-Salen complex displayed a well-defined peak at 20 mV. The in-situ method (IM) voltammogram was tested by mixing equimolar amounts of cobalt ion and Salen ligand for 900 s and scanned from -1.5 to 1.8 V. The oxidation scan provided peaks similar to the cobalt-Salen complex confirming that complexation between cobalt and Salen took place.

In ex-situ method (EM), the Naf-Sal@ GCE was immersed into the EC cell containing 2.5 x 10^{-4} M cobalt ion in buffer solution. The oxidative scan was run with a deposition time of 900 s. All peaks resemble the cobalt-Salen complex with the main complex peak present at 20 mV confirming that the complex was formed on the GCE's electrical double layer (Figs. 22 and 23).

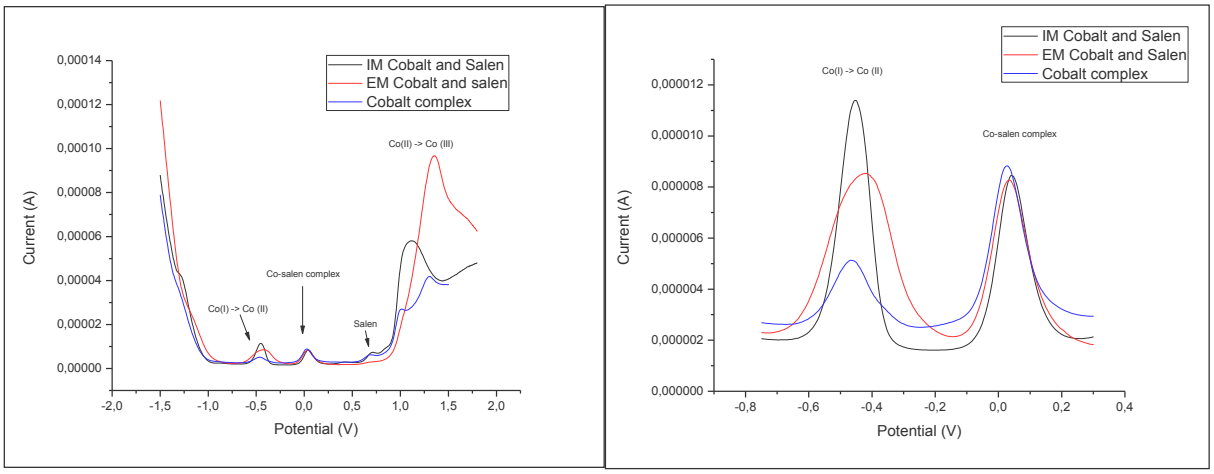

Figure 22: SQW oxidative voltammogram of cobalt-Salen complex at bare GCE, (IM) of Co and Salen at bare GCE and (EM) of Naf-Sal@GCE with Co.

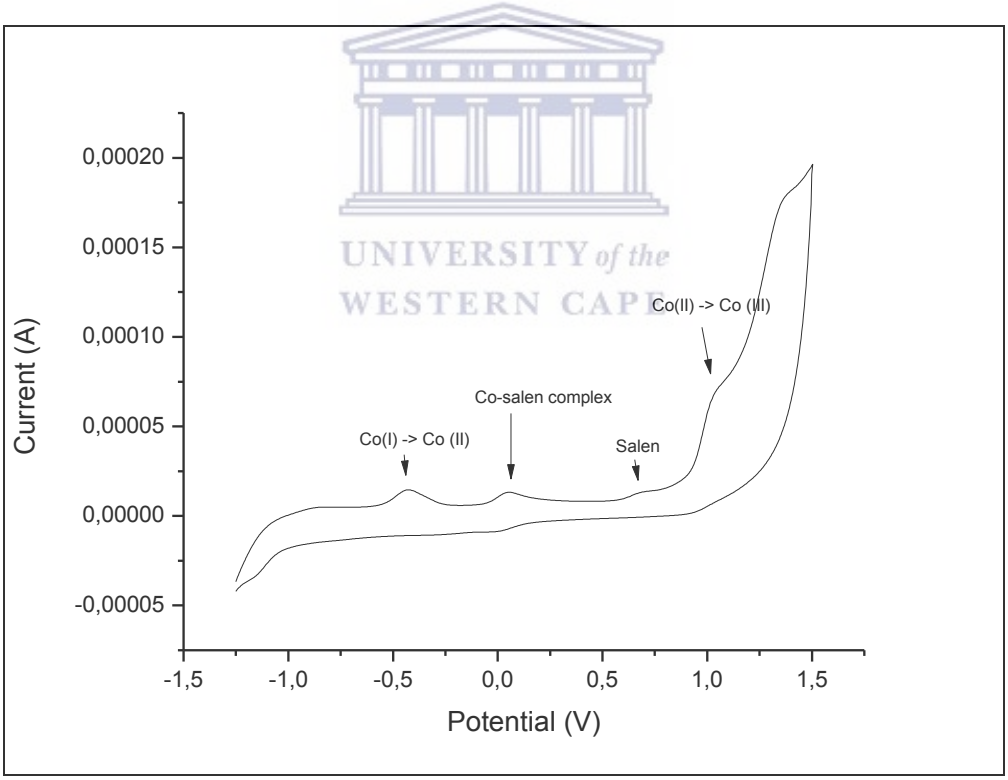

Figure 23: CV scan of cobalt-Salen complex at bare GCE

Electrode modification via the Ex-situ method (EM)

The Ex-situ mixing method as discussed in, Chapter 3, involves the extraction of heavy metal ions using a modified electrode. The glassy carbon electrode was modified with the Salen ligand, RGO-Salen and with the Naf-Salen ink as shown in Figure 24.

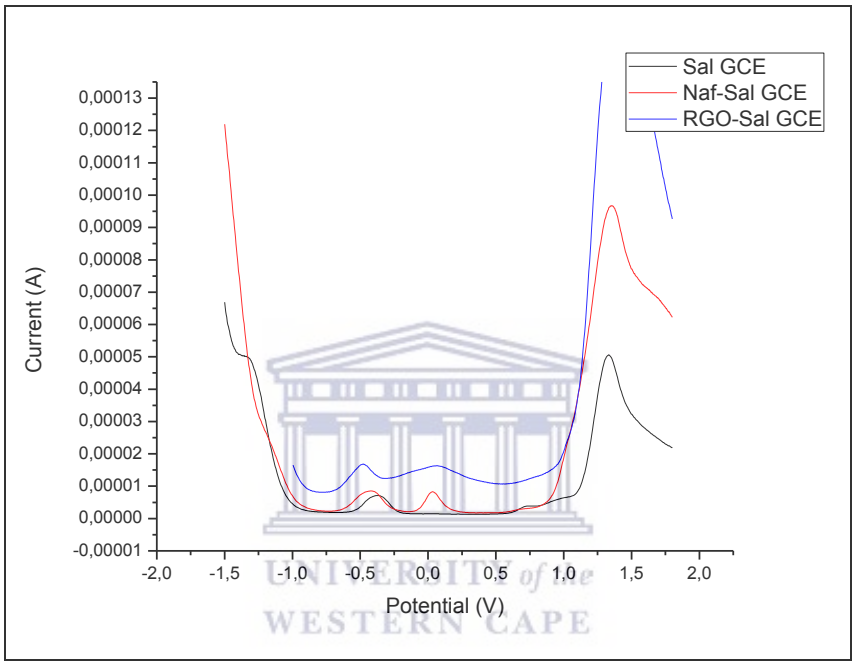

Figure 24: Comparison of SQW oxidative voltammogram for EM using Sal, Naf-Sal and RGO-Sal/GCE at 2.5 x 10^{-4} M Co

The Salen modified GCE was tested for the removal of cobalt ion (2.5 x 10^{-4} M) in the buffer solution. The SQW voltammogram, showed that the cobalt was unable to complex with the Salen ligand on the electrode surface as no peak for the complex was observed.

The RGO-Sal@GCE was prepared by reducing the graphene oxide electrochemically onto the glassy carbon surface as described in Chapter 3. The RGO modified electrode was allowed to dry and 2µL of 5 x 10^{-3} M Salen was drop-casted forming the RGO-Sal

modified GCE. This electrode was tested for its extraction ability to remove cobalt ions via complexation at the electrode surface. The results proved that the RGO-Sal was successful in complexing with cobalt ion confirmed by the appearance of complex oxidation peak at 20 mV.

The Naf-Sal@GCE modified electrode prepared by coating the electrode with a Nafion-Salen ink was immersed into the electrochemical cell containing the metal ion of interest. Square-wave voltammetry oxidation scan was applied to extract the cobalt metal ion from the buffer by forming a complex at the electrode surface. This complexation was observed by the oxidation peak at 20 mV in the voltammogram above.

It can be concluded that for the ex-situ method, the modified electrode Naf-Sal@GCE demonstrated the most distinct and well-defined peak for the extracted heavy metal ion.

Extraction of heavy metal ions studies by ex-situ method

Calibration curve of EM of Cobalt ions with Naf-Sal@GCE

The calibration curve was constructed to evaluate the effect of concentration of the solution (Fig. 25) by adding certain concentrations of cobalt metal ion. These cells were purged for 300 s and then a SQW oxidative scan was run using Naf-Sal@GCE (2µL of the Salen-nafion ink was precisely drop casted onto the GCE surface to ensure reproducibility). The parameters of the scan were set to run the potential from -1.5 to 1.5 V at a deposition time of 600 s for each run. The result showed that on increasing the concentration from 100 ppb to 40 ppm, the cobalt-Salen complex peak increased until it reached a certain concentration (30 ppm) where oversaturation of the electrode surface occurred.

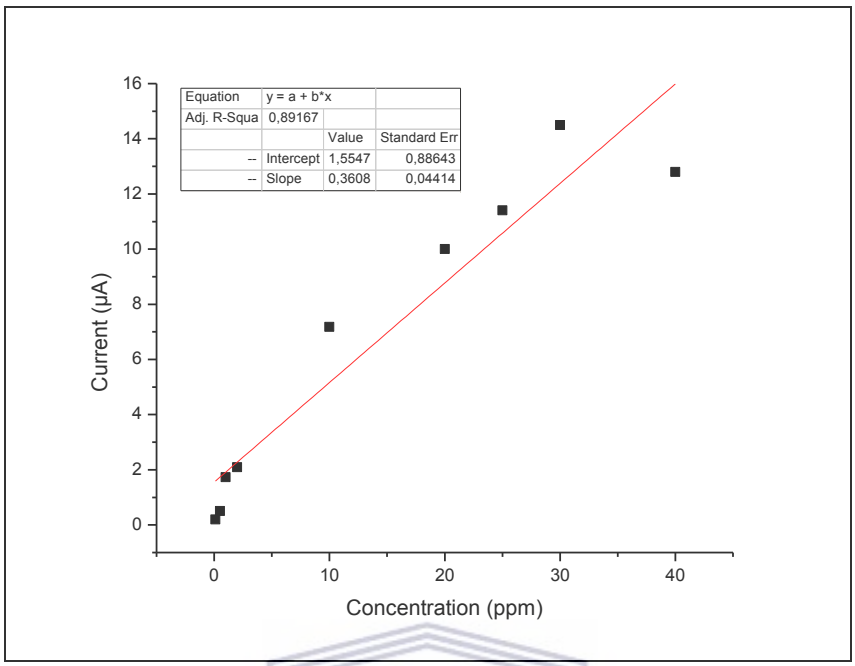

Figure 25: Calibration curve of EM of cobalt ions with Naf-Sal@GCE

From the calibration curve, the equation of the graph is

$$y = 0.3608x + 1.5547 \qquad \textbf{Equation 4}$$

From this equation, the peak height used to determine the extracted concentration of the

Determination of unknown metal ion concentration

An unknown concentration of cobalt metal ion was added to the electrochemical cell via the Ex-situ mixing and the metal ion was extracted via complexation on the Naf-Sal@GCE surface. The electrode was then removed, rinsed lightly with ultrapure water and allowed to dry. The electrode containing the extracted metal was then immersed into a clean phosphate buffer solution and the complex was stripped off (Fig. 26). The

resulting peak height was in tandem with the calibration curve above to determine the extracted amount of metal ion by applying equation 4.

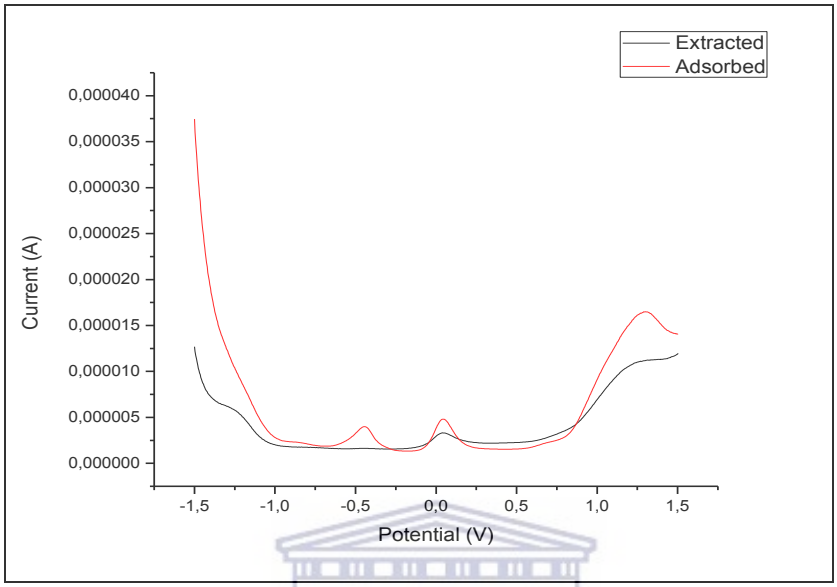

Figure 26: Extraction of unknown sample

Calculation

$y = 0.3608x + 1.5547$

$x = \frac{y}{0.3608} - 1.5547$, where y = peak height = 1.32 µA

$x = \frac{1.32}{0.3608} - 1.5547$

$x = 2\ ppm$

Therefore, the unknown extracted metal ion concentration was found to be 2 ppm.

Extraction percentage

Extraction percentage (%) = $\frac{C_i - C_f}{C_i}\ x\ 100$

from

Figure **26** the

$$\textbf{extraction percentage} = \frac{3.41\ \mu A - 1.32\ \mu A}{3.41 \mu A}\ x\ 100 = 61\%$$

Factors affecting the removal efficiency of metal ions

Effect of concentration

The effect of cobalt concentration on the percentage removal via the ex-situ method is shown in Figure 27. It is clear the adsorption capacity increases as the concentration increases until it reaches a plateau where the electrode becomes oversaturated.

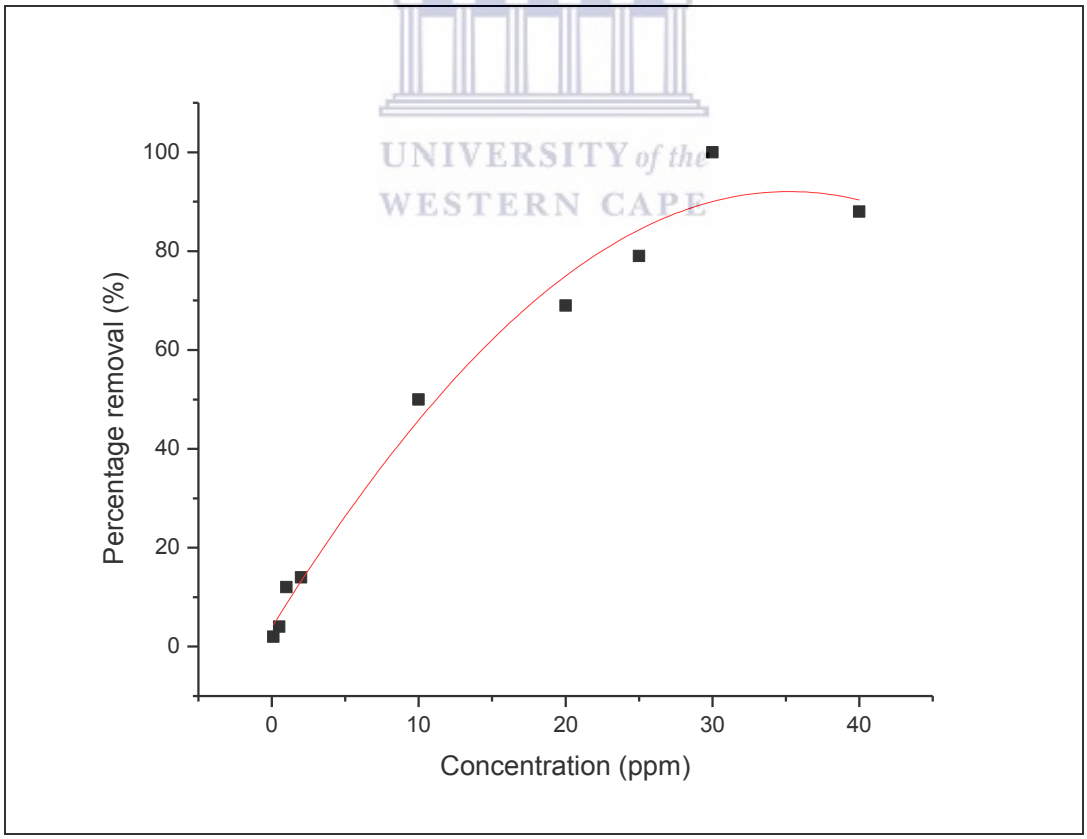

Figure 27: Effect of concentration on % removal of Co ion

Effect of accumulation time

Figure 28 demonstrates the influence of deposition time on the peak currents for the extraction of Co ions using Naf-Sal@GCE. The deposition time was varied from 0 to 900 s at 150 s increments. The cobalt-Salen complex peak current, through the stripping responses of the metals, steadily increases with increasing deposition time from 0 to 750 s, thereafter the detection limit starts decreasing due to the saturation of the electrode surface. Therefore, a deposition time of 600 s was selected for all subsequent experimentation ensuring that the peak of the complexes is enhanced using the ex-situ method and to avoid possible saturation of the electrode surface.

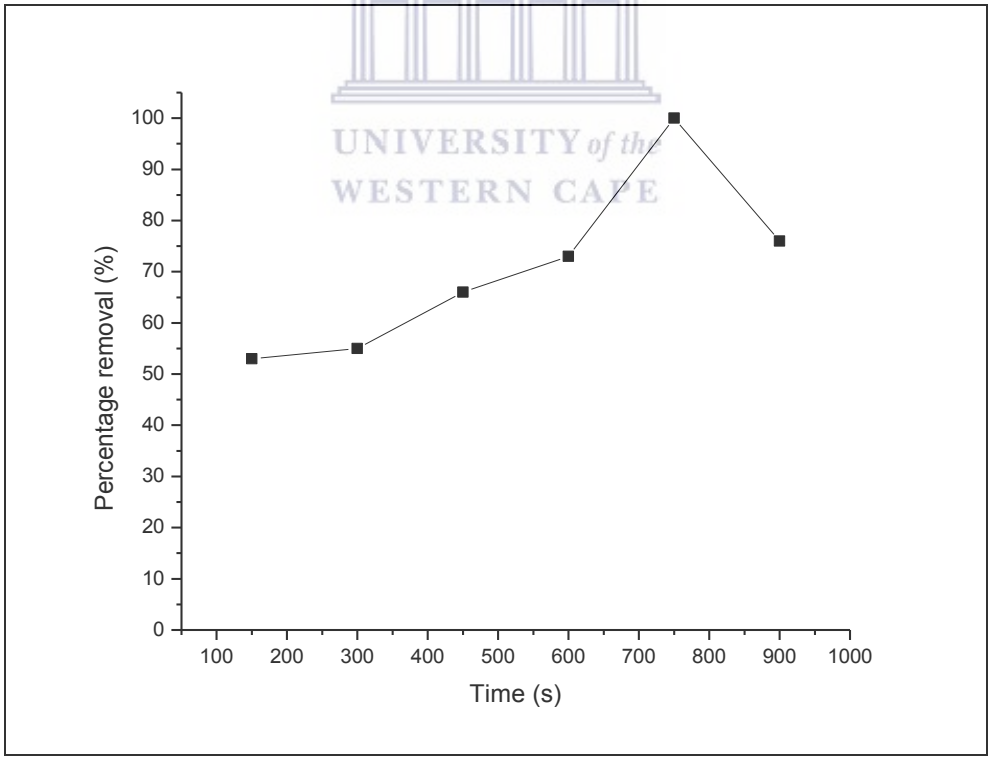

Figure 28: Effect of deposition time on % removal of Co ions

Effect of buffer solution

The effect of varying buffer solutions via the ex-situ method was investigated to determine the best buffer medium for the analysis. The type of the buffer solution was varied while keeping all other parameters fixed throughout the process. The EM method was run with 2.5 x 10^{-4} M of Co in the buffer solutions.

Three buffer solutions were used in this study. The results illustrated (Fig. 29) that using an ammonia-ammonium buffer chloride solution (0.1M, pH 9.66), complexation did not take place at high pH since the concentration of hydroxyl ion hinders the adsorption of metal ions on the electrode surface for complexation [96].

On using an acetate buffer (0.1 M, pH 4.6), active sites on the adsorbent material are H^+ ions. The metal i.e. Co of the complex is reduced resulting in increasing the current. Using a phosphate buffer (0.1 M, pH 7.2) an increase in $Co(OH)_2$ and a decrease in Co(II) ions result which are easier to oxidize to $Co(OH)^+$. Therefore, the phosphate buffer was chosen as the optimum buffer solution for all experiments.

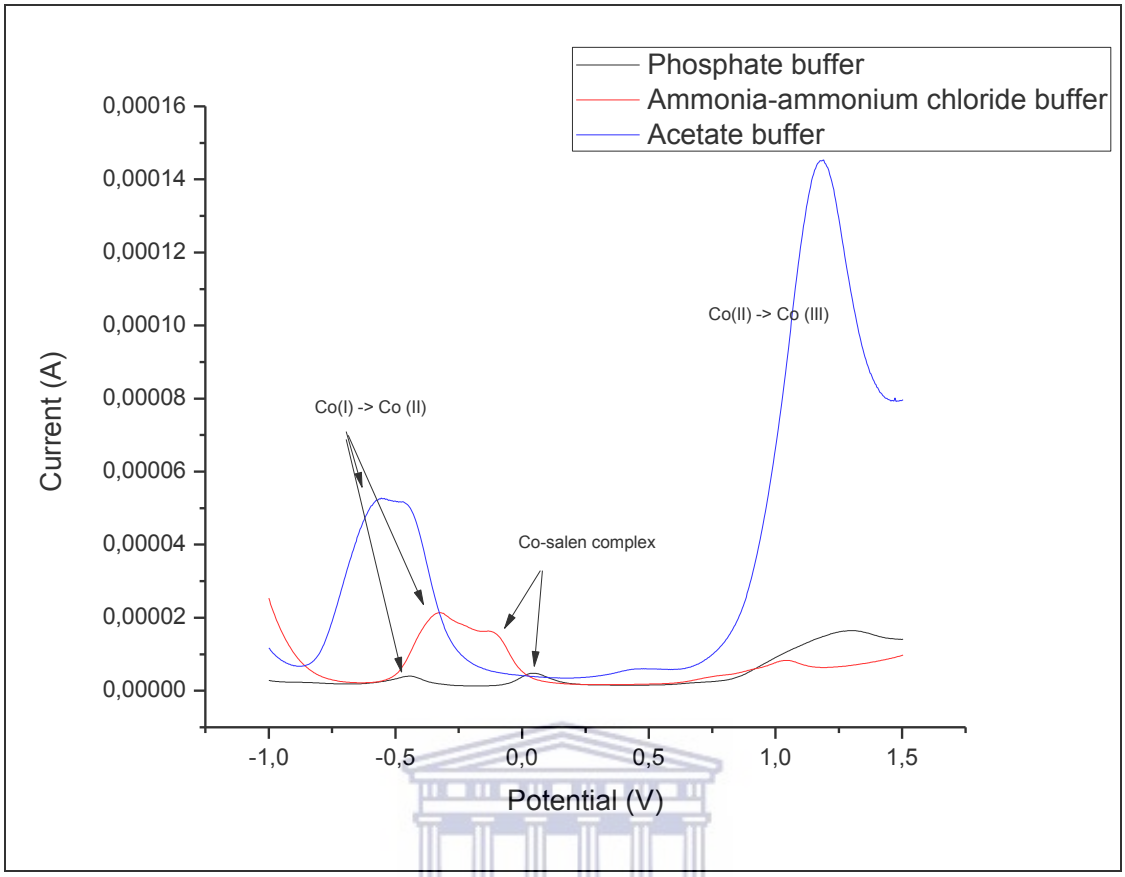

Figure 29: Effect of various buffer solutions on ex-situ mixing of Naf-Sal@GCE with cobalt

Reusability

Reusability studies were performed using the Naf-Sal modified GCE to test whether the electrode could be reused after extraction of the metal ions and subsequent stripping off of the metal in a fresh clean buffer solution. The electrode was then re-immersed into the cobalt containing buffer solution and the ex-situ method was applied. It was determined that the electrode was not reusable and had to be prepared over successive experimentation.

Extraction of heavy metal ions studies by the in-situ method

Calibration curve of Cobalt ion and Salen using IM

Extraction studies were also performed using the in-situ method. A calibration curve was constructed by varying the concentration of the cobalt ions from 100 ppb to 15 ppm while fixing the Salen concentration at 20 ppm and deposition times of 600 s and 150 s, respectively (Fig. 30). Square wave voltammetry was performed from -1.5 V to 1.5 V for each scan. The result showed that as the concentration of cobalt increased the peak height (current) of the complex increased linearly until the electrode became oversaturated (curve flattened out). From the graph, a straight line was drawn to determine the concentration of an unknown extracted sample.

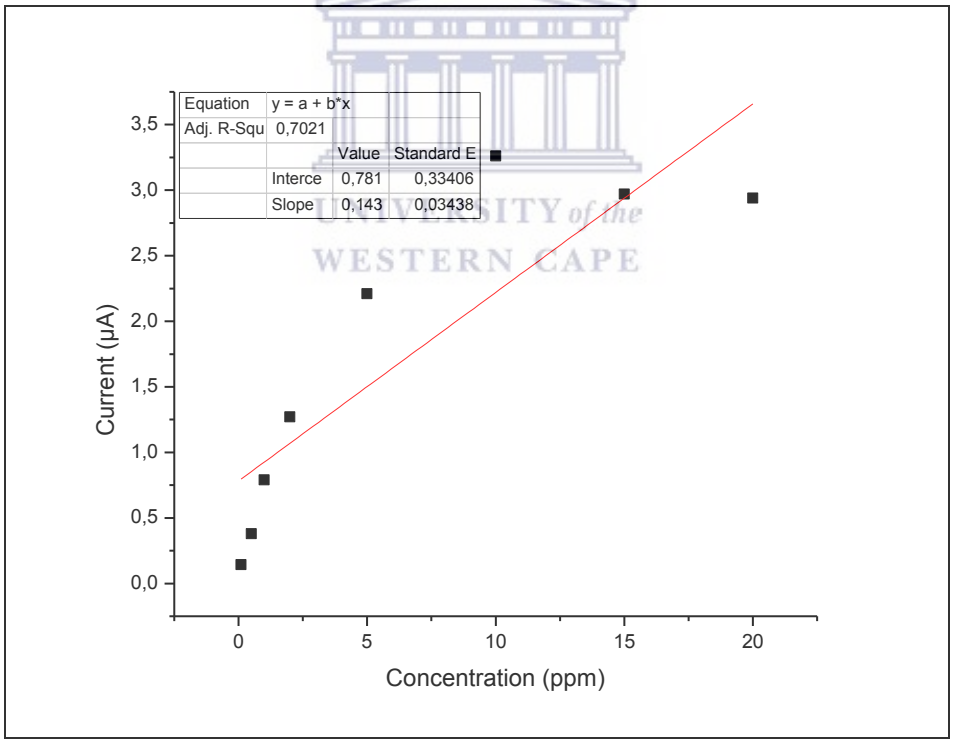

Figure 30: Calibration curve of cobalt and Salen using (IM)

The equation of the graph as extrapolated is

$$y = 0.143x + 0.781 \qquad \textbf{Equation 5}$$

Determining unknown concentration

An unknown concentration of metal ion was added to the cell containing 20 ppm Salen at in-situ conditions, and the electrode was removed and rinsed lightly. The same electrode was then immersed into an EC cell containing fresh buffer and square wave and an oxidative scan was run. The resulting voltammogram was recorded and the height of the complex peak was obtained (0.356 µA). The obtained result was used to determine the amount of metal extracted according to the following calculations.

Calculation

$y = 0.143x + 0.781$

$x = \frac{y}{0.143} - 0.781$ where y = peak height = 0.356 µA

$x = \frac{0.356}{0.143} - 0.781$

$x = 1.7\ ppm$

Therefore, the calculated concentration of the unknown sample which was extracted is 1.7 ppm.

Removal efficiency

Effect of concentration

The effect of cobalt concentration on the removal efficiency for the in-situ method was studied and shown in Figure 31. The graph depicts that a linear relationship was obtained up to 10ppm of Co concentration indicating that as the concentration increases, the amount of metal extracted increases i.e. current peak intensifies. The detection limit starts decreasing after 10ppm concentration. This is due to saturation of the electrode surface.

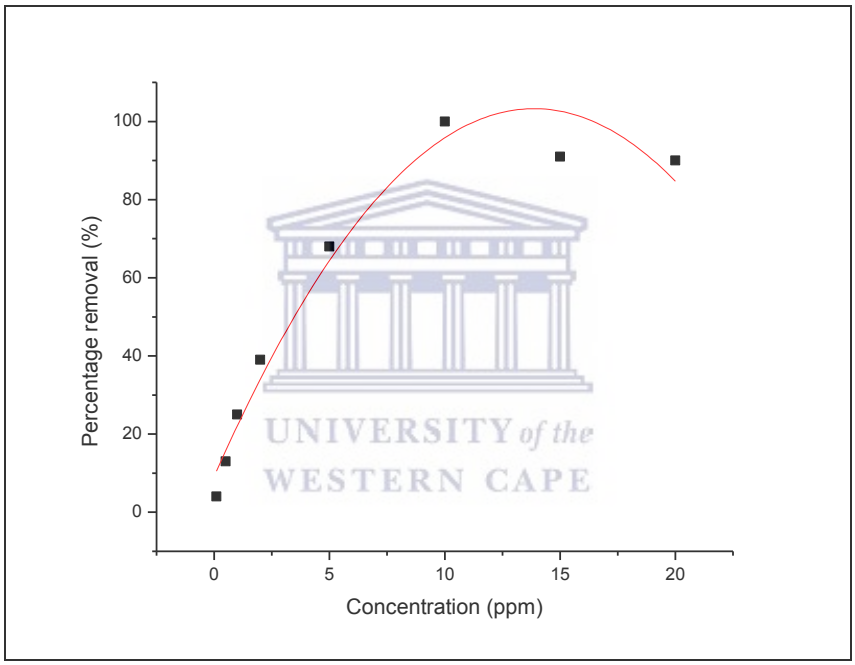

Figure 31: Effect of concentration on % removal of cobalt ion

Effect of accumulation time

The effect of deposition time using the in-situ method was investigated by varying the deposition time from 0 to 900 s at 150 s increments while fixing a concentration of 2 ppm and 10 ppm for cobalt and Salen, respectively. Square wave voltammetry was undertaken

from -1.5 to 1.5 V for each run. The results indicated that increasing the deposition time had a negligible effect on the complexation between the metal and ligand.

Electrochemical study of the Salen ligand and nickel complex

In order to study the % removal of heavy metal ions, nickel was selected for complexation with Salen. Figure 32 shows an oxidation peak position of Ni(II) ion (2.5 x 10^{-4} M) at -270 mV (inset).

The SQW voltammogram (Fig. 33) shows the oxidation peaks for the Ni-complex at -270 mV, 850 mV and 1.25 V which are assigned to nickel, the Salen ligand, and the nickel-Salen complex, respectively. It is evident from the figure that the oxidations peaks are clearly observed while the reduction peaks are not that pronounced. Hence, this work focuses mainly on the oxidation sweep region of the Salen complexes.

For the in-situ mixing (IM), equimolar quantities of Salen and nickel ion were added to the electrochemical cell. The cell was allowed to stir for 900 s for complexation to occur and the SQW voltammetric oxidation scan was run from -1.5 to 1.8 V. The voltammogram displayed similar results to the nickel-complex showing peaks at -250 mV, 829 mV and 1.31 V confirming that nickel-Salen complexation was successful. On the other hand, the ex-situ mixing method (EM) was used to form the nickel-Salen complex on the electrode surface. The electrode surface, which was modified using the Naf-Sal ink, was immersed into the EC cell containing 2.5 x 10^{-4} M nickel ions. The cell was purged for 300 s and the SQW oxidation scan was run from -1.5 to 1.8 V at a deposition time of 600 s. with slight shifting as the metal is harder to oxidize on the GCE surface The oxidation peak positions are observed at -240 mV, 750 mV and 1.6 V for

nickel, Salen and nickel-Salen complex, respectively. The peaks observed via (IM) and (EM) were comparable to the nickel-Salen complex with slight shifting as the metal is harder to oxidize on the GCE surface.

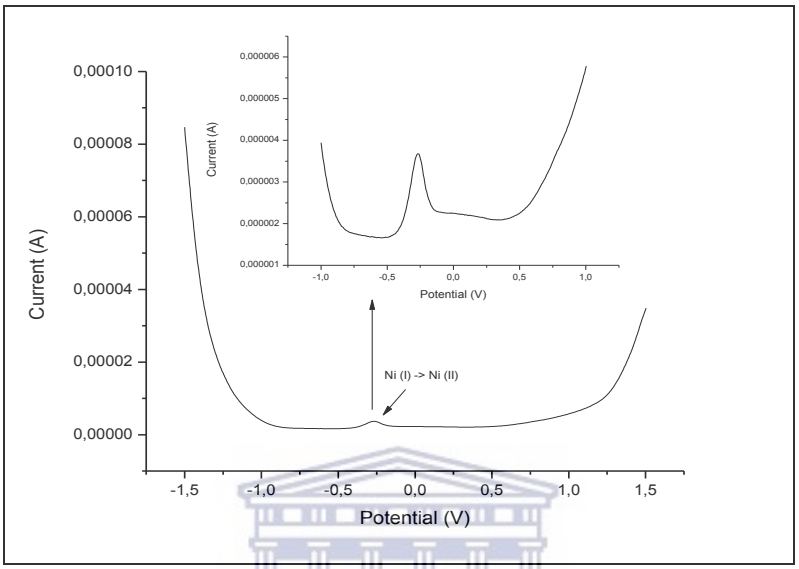

Figure 32: SQW Voltammogram Nickel of (2.5 x 10^{-4} M) at bare GCE with expanded region (inset)

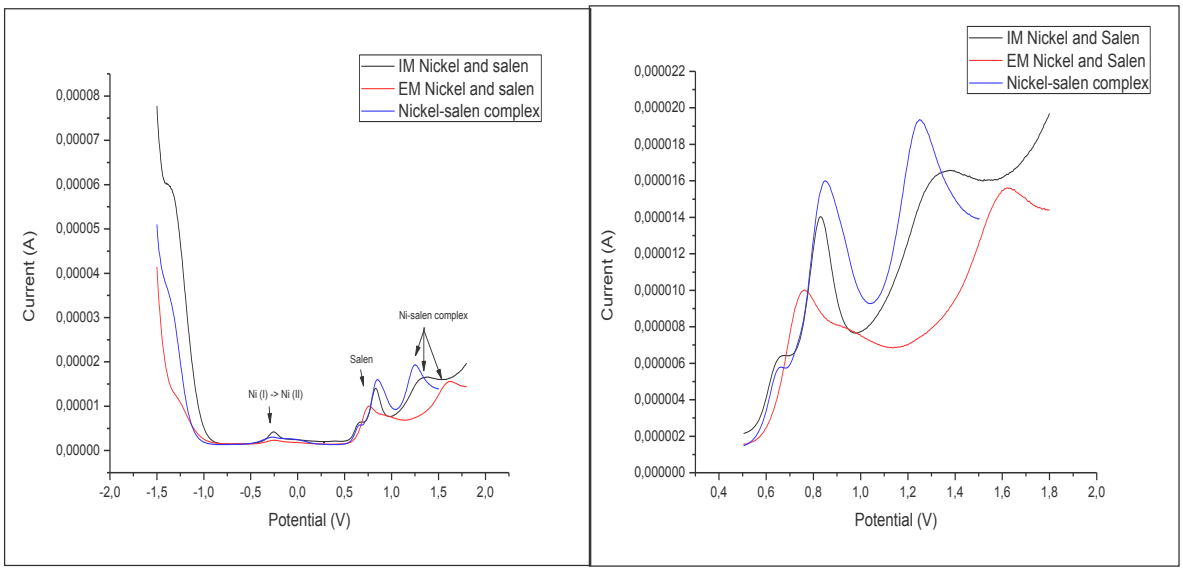

Figure 33: SQW oxidative voltammogram of nickel-Salen complex at bare GCE (blue), (IM) (black) and (EM)(blue), (left), Expanded region (right)

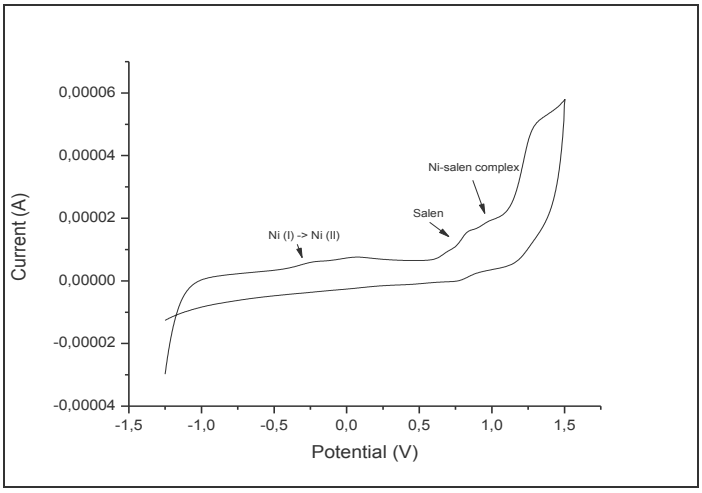

Figure 34: Cyclic voltammogram of nickel-Salen complex (2.5 x 10^{-4} M) at bare GCE

SQW of Salen ligand and Copper ion

Figure 35 shows the oxidation peak position for the copper metal ion. The peak is observed at a potential of -90 mV. The copper-Salen complex (2.5 x 10^{-4} M) was analysed by CV and SQW (Figs. 36 and 37). The oxidation peaks for the copper metal ion and Salen are observed at -100 and 870 mV while a new peak was observed at 130 mV due to the copper-Salen complex.

For the IM method (Fig. 37), 1 x 10^{-5} M copper metal ion and 2.5 x 10^{-4} M Salen were added to the buffer and stirred for 900 s. The oxidation scan showed the copper metal ion and Salen peaks indicating that no complexation had occurred.

The EM voltammetric scan consisted of the Naf-Sal@GCE immersed into the EC cell containing 1 x 10^{-5} M copper metal ion in the buffer solution. The oxidation voltammogram showed no new peaks related for the copper-Salen complex formation. It can thus be concluded that complexation was not achieved by both in-situ or ex-situ methods (Fig. 37).

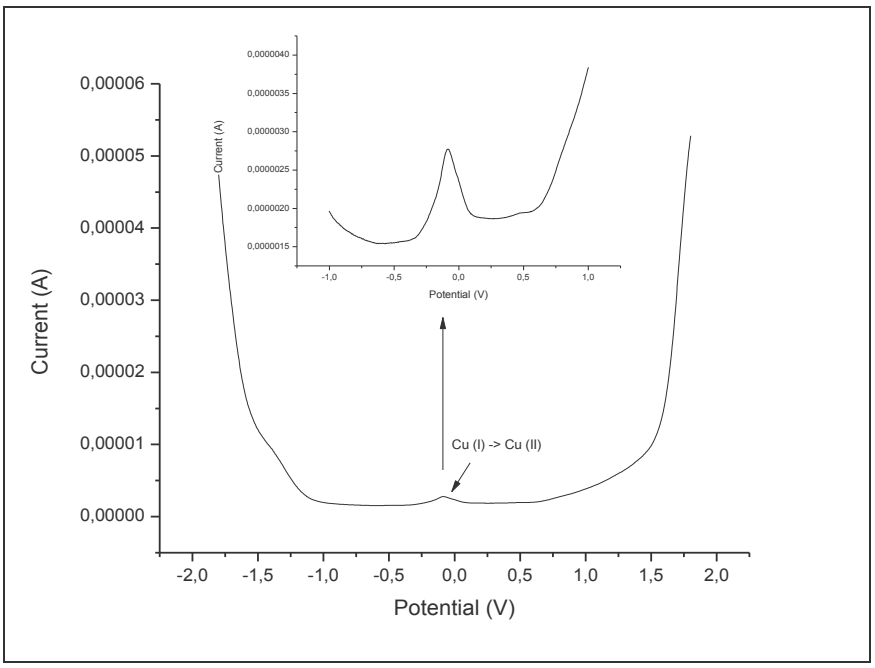

Figure 35: SQW of oxidation scan of copper metal ion (2.5 x 10^{-4} M) at bare GCE, (inset) expanded region

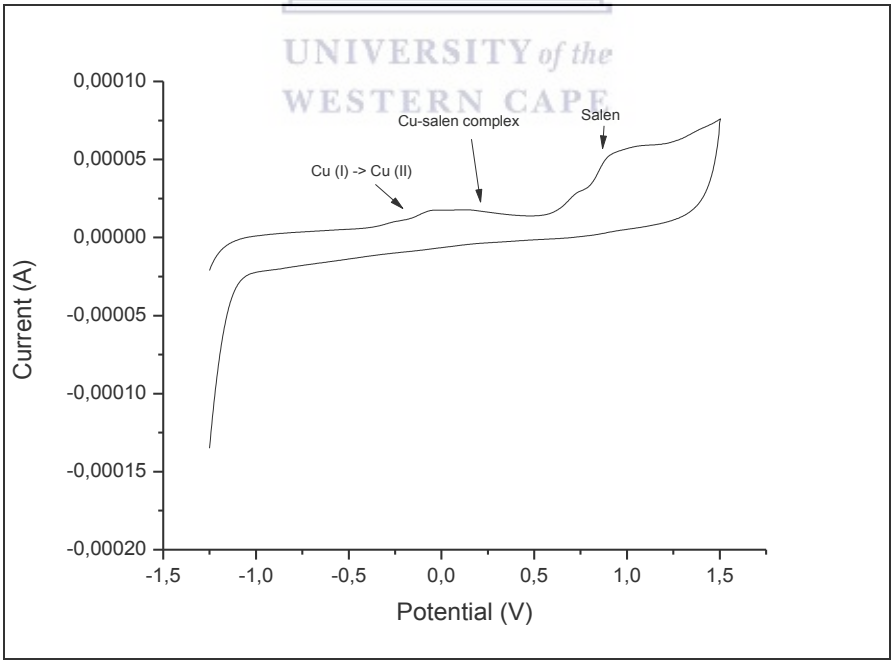

Figure 36: CV of copper-salen complex (2.5 x 10^{-4} M)

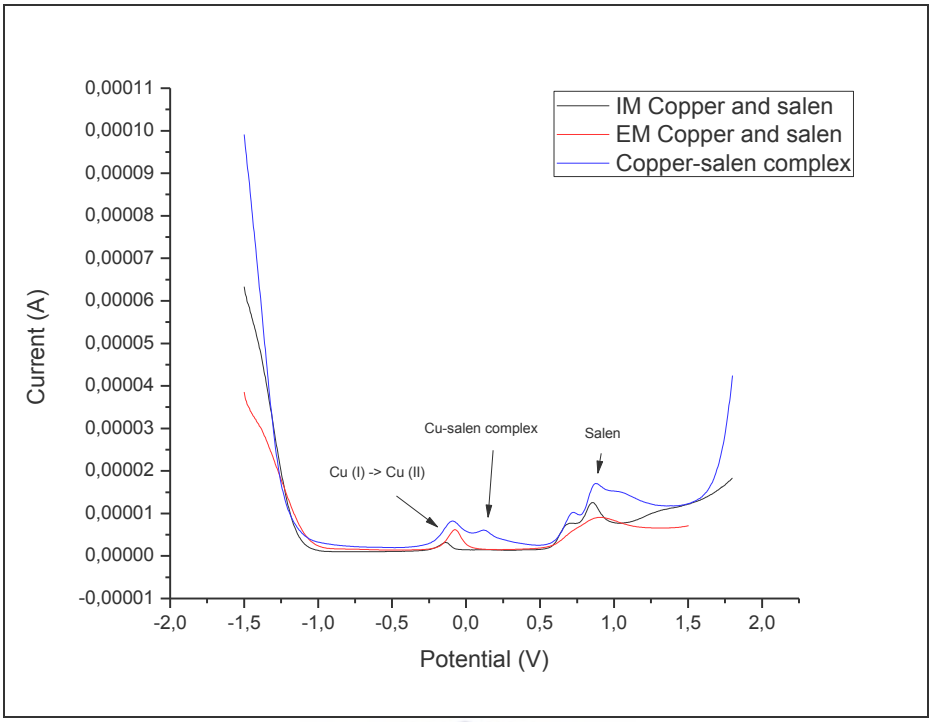

Figure 37: SQW oxidative voltammogram of Cu-Salen complex at bare GCE, in-situ mixing of Cu and Salen at bare GCE and ex-situ mixing of Naf-Sal@GCE with copper

CHAPTER 5: RESULTS AND DISCUSSION:

5.1 Introduction

This chapter involves the synthesis and characterisation of 1,3-bis(salicylideneamino)-2-propanol abbreviated as Sal-DAP. The ligand was identified using various techniques including FTIR, ^{1}H, ^{13}C NMR and GC-MS. This ligand was used as a chelating agent for the removal of heavy metal ions by electrochemical methods discussed in this chapter.

Sal-DAP ligand

Sal-DAP ligand was characterized using ATR-IR to confirm its structure and the functional groups present. The IR spectrum shown in Figure 38 displays a strong broad band at 3380 cm^{-1} which is assigned to the O-H bond. The C-H bands of aromatic rings and from the methylene CH_2 groups are present as weak bands at 3062, 3010 and 2895 cm^{-1}. The azomethine group appeared as strong band at 1631.5 cm^{-1} which confirms the formation of the ligand. The medium peaks between 1578.3 to 1439.5 cm^{-1} are assigned to CH groups bending as well as C=C and =C-H stretching vibrations. Medium to strong bands being observed between 1274.2 and 1025.7 cm^{-1} are assigned to CH_2 bending and C-O and C-C stretching. The peaks at 855.6 and 749.9 cm^{-1} are due to the aromatic ring vibrations. The disappearance of the NH_2 stretching vibration peak confirmed the formation of the ligand.

The FTIR of metal-Sal-DAP complexes showed characteristic peaks such as a strong peak at 1470-1479 cm^{-1} assigned to the C=C stretching vibration. The shift in the C=N streching peak to lower frequency (1628-1625 cm^{-1}) indicates coordination of the nitrogen of azomethine to metal. New medium bands at 473 and 476 cm^{-1} are observed due to M-N bonds for the nickel and copper, respectively.

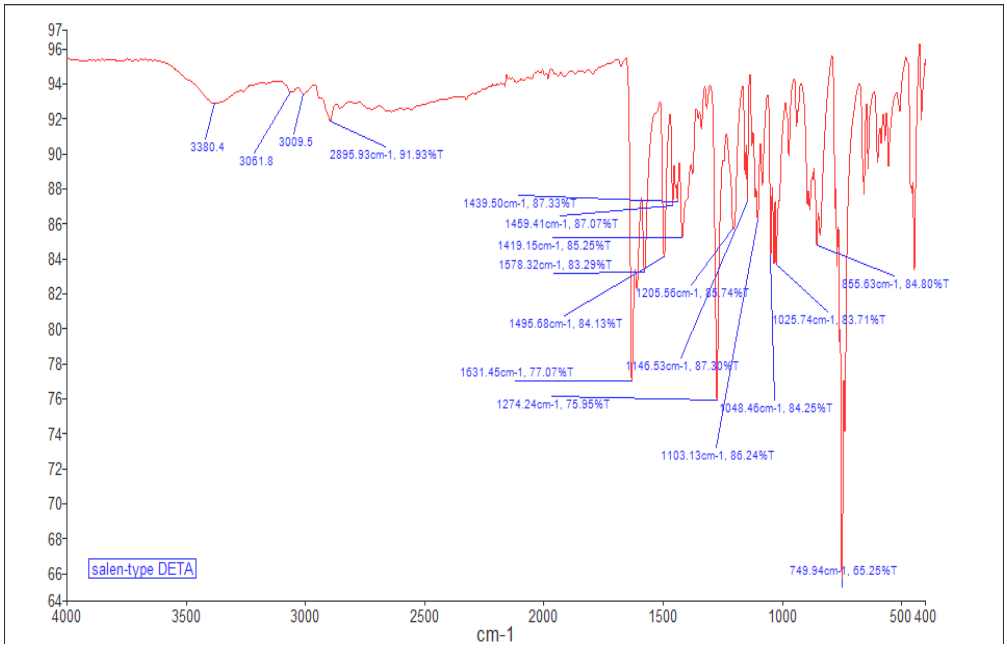

Figure 38: FTIR spectrum of Sal-DAP ligand

Metal complexes of Sal-DAP

Nickel-Sal-DAP complex

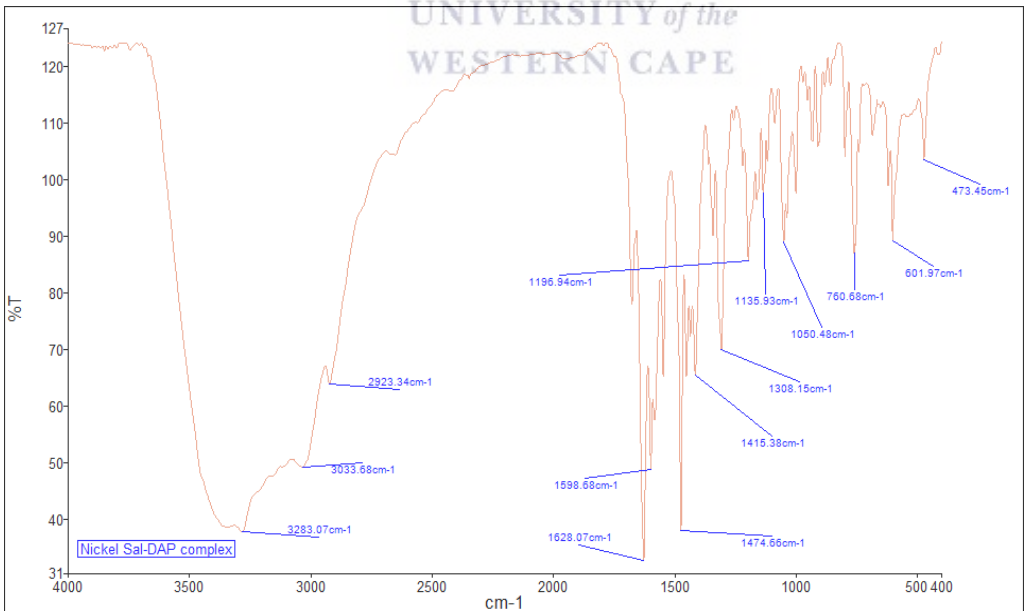

Figure 39: FTIR Spectrum of Ni-Sal-DAP complex

Copper-Sal-DAP complex

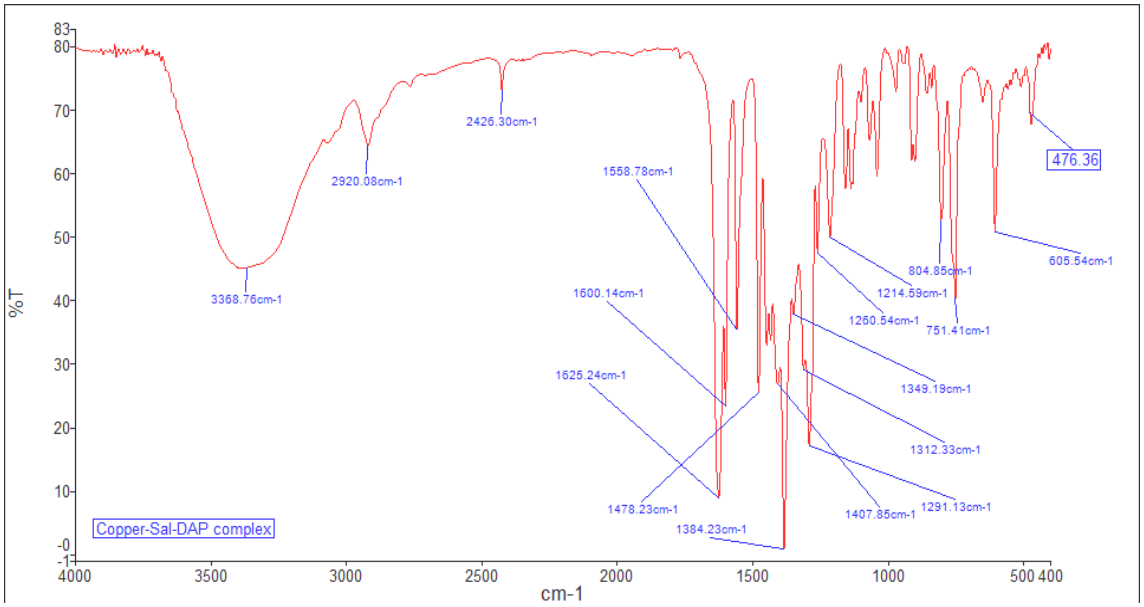

Figure 40: FTIR Spectrum of Cu-Sal-DAP ligand

Cobalt-Sal-DAP complex

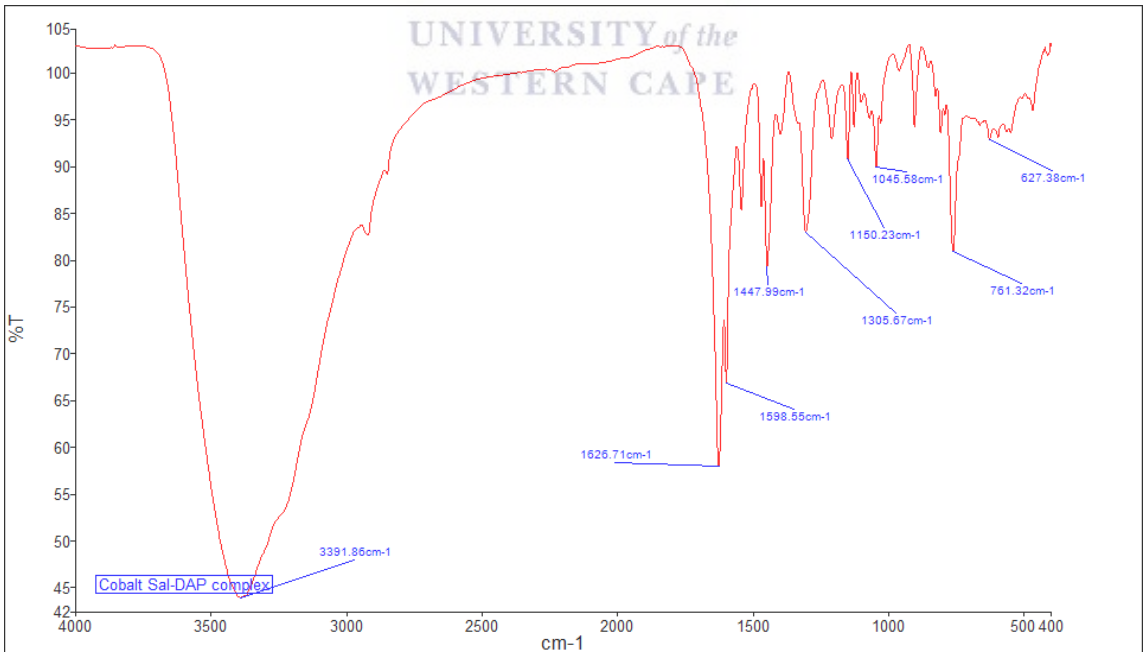

Figure 41: FTIR Spectrum of Co-Sal-DAP complex

5.2 GC-MS

GC-MS confirms the formation of Sal-DAP ligand by the peak at 298.3 m/z for the molecular ion of the ligand (Fig. 42).

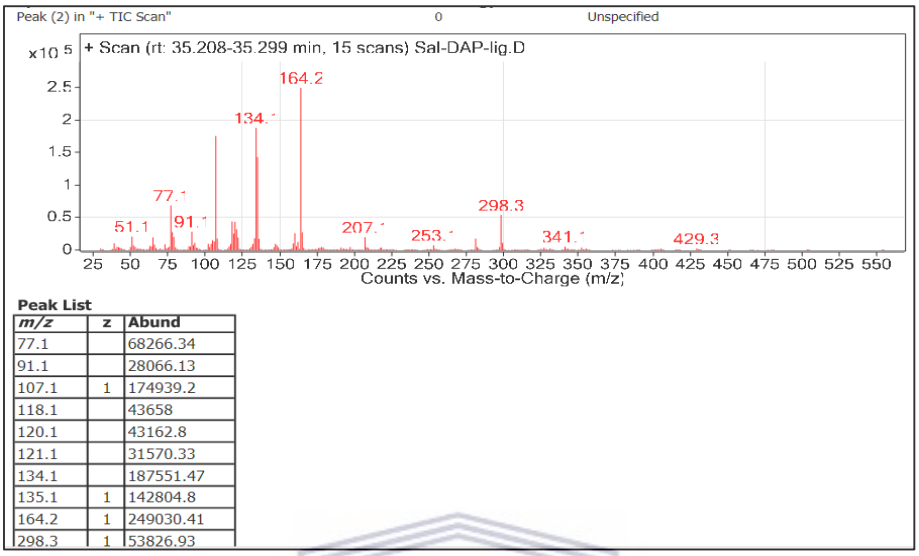

Peak List

m/z	z	Abund
77.1		68266.34
91.1		28066.13
107.1	1	174939.2
118.1		43658
120.1		43162.8
121.1		31570.33
134.1		187551.47
135.1	1	142804.8
164.2	1	249030.41
298.3	1	53826.93

Figure 42: GC-MS chromatogram of Sal-DAP ligand

5.3 NMR

^{1}H NMR

The ^{1}H NMR spectrum of the ligand is shown in Figure 43. The broad signal at 13.19 (br s, 2H) ppm is assigned to phenolic -OH protons. The aliphatic -OH proton showed a peak at 4.24 (br s, 1H) ppm. The aromatic hydrogens peaks are at 7.30 (dt, 2H), 7.23 (d, 2H)), 6.94 (dt, 2H) and 6.86 (d, 2H) ppm. The proton of -CH=N appears as a peak at 8.36 (s, 2H) ppm. The peaks at 3.82 (d, 1H) and 3.68 (m, 4H) ppm are assigned to the protons attached to the alcoholic carbon and methylene groups, respectively.

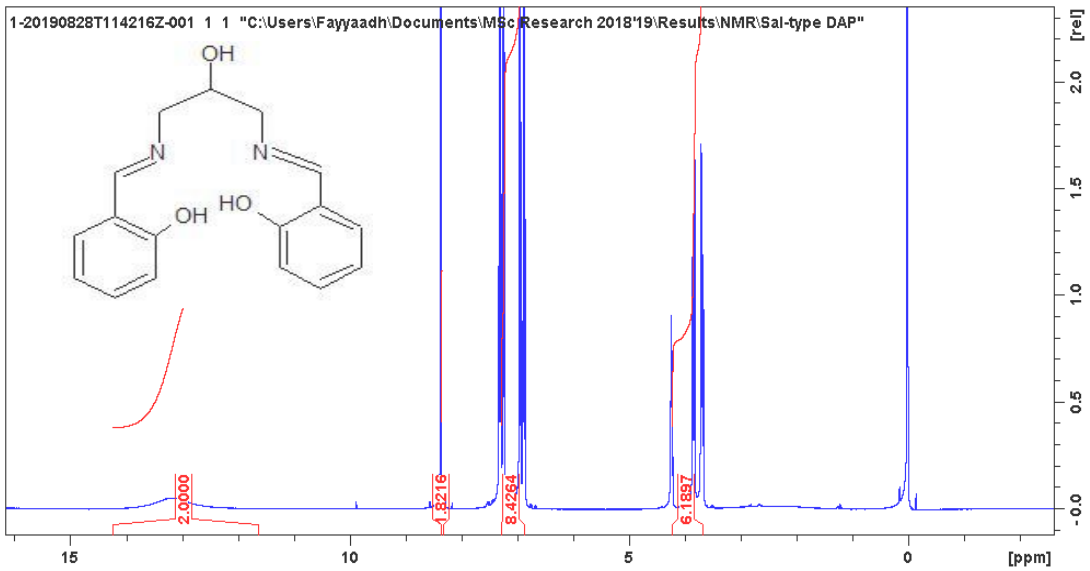

Figure 43: ^{1}H NMR spectrum of Sal-DAP ligand dissolved in $CDCl_3$ using 400 MHz NMR instrument

^{13}C NMR

The ^{13}C NMR spectrum is shown in Figure 44. The signal at 167.37 ppm is assigned to the C-OH of the phenolic systems. The C=N peak appeared at 161.15 ppm, the peaks of aromatic carbons observed at 132.69, 131.73, 118.75, 118.59 and 117.31 ppm. The CH_2 group showed a signal at 63.10 ppm while CH(OH) peak appeared at 70.68.

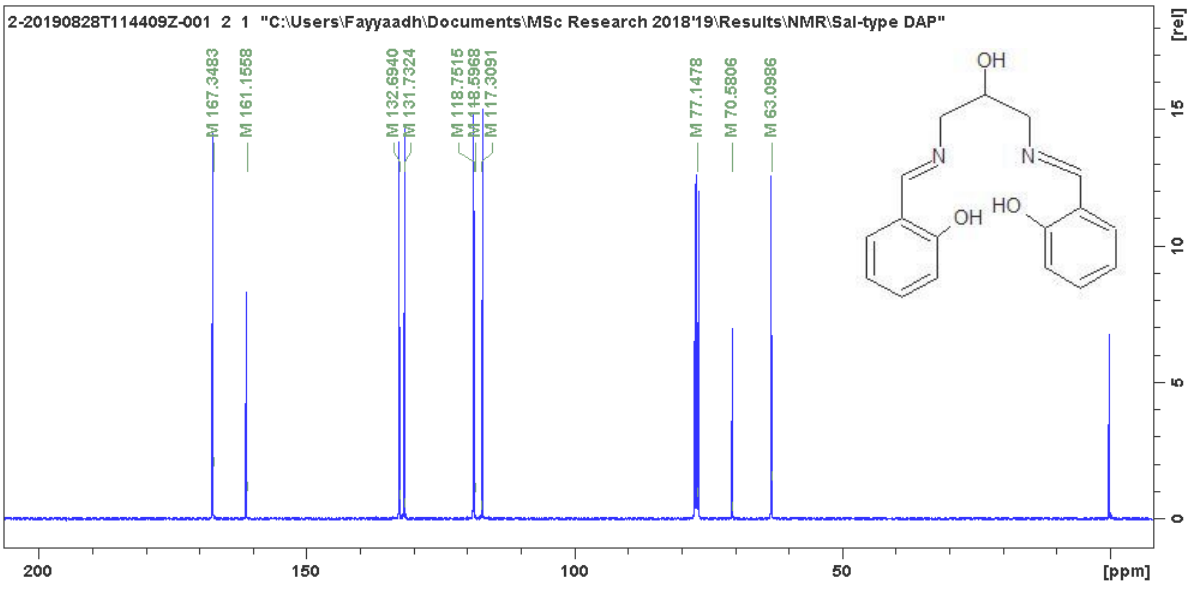

Figure 44: ^{13}C NMR spectrum of Sal-DAP ligand in $CDCl_3$ using 400 MHz NMR instrument

5.4 Electrochemical studies Characterisation

Sal-DAP and Naf-Sal-DAP GCE

A solution of the Sal-DAP ligand (2.5 x 10^{-4} M) was electrochemically investigated to determine its oxidation peaks in phosphate buffer solution. SQW was scanned from -1.5 to 1.8 V and showed an oxidation peak at 850 mV with a shoulder at 660 mV.

SQW voltammetry of Naf-Sal-DAP GCE in a phosphate buffer solution was scanned from -1.5 to 1.8 V with a deposition time of 600 s and showed an oxidation peak at 940 mV (Fig. 45).

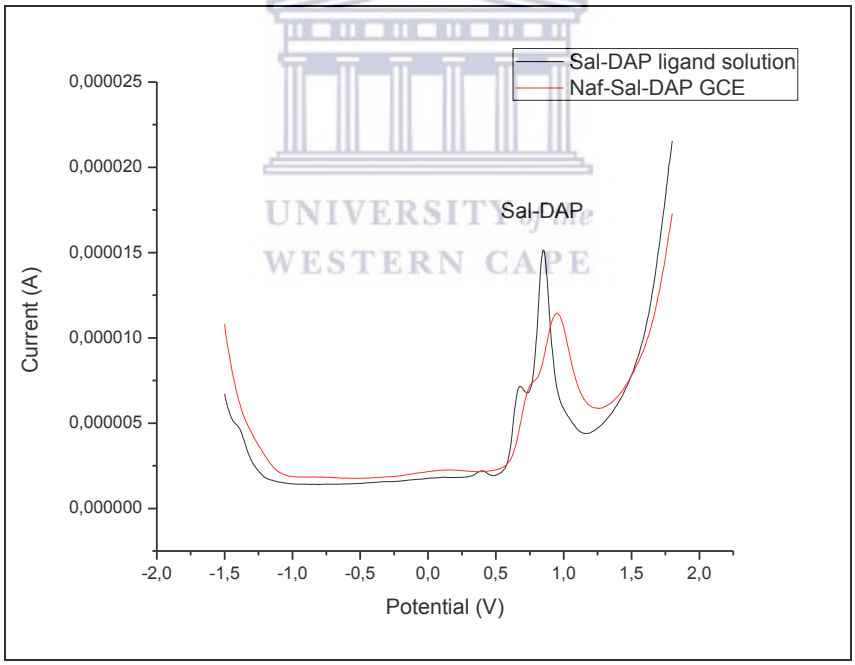

Figure 45: SQW oxidative voltammogram of Sal-DAP (2.5 x 10^{-4} M) and Naf-Sal-DAP@ GCE in buffer solution

SQW of Nickel metal ion and Sal-DAP

Figure 46 shows SQW of nickel metal ion where the oxidation peak was positioned at -270 mV. The voltammograms of the Ni-Sal-DAP complex bare along with the complex via IM and EM is shown in Figure 47. The SQW voltammetry of in-situ method was achieved by mixing equimolar amounts of Nickel ion and Sal-DAP ligand in the buffer and allowed to stir for 900 s. The oxidation peaks were found to be similar to the Ni-Sal-DAP complex confirming that complexation took place. The Nickel peak appeared at -290 mV and sal-DAP peak at 710 mV. A new peak was observed at 1400 mV for Ni-Sal-DAP complex which confirmed the complex formation.

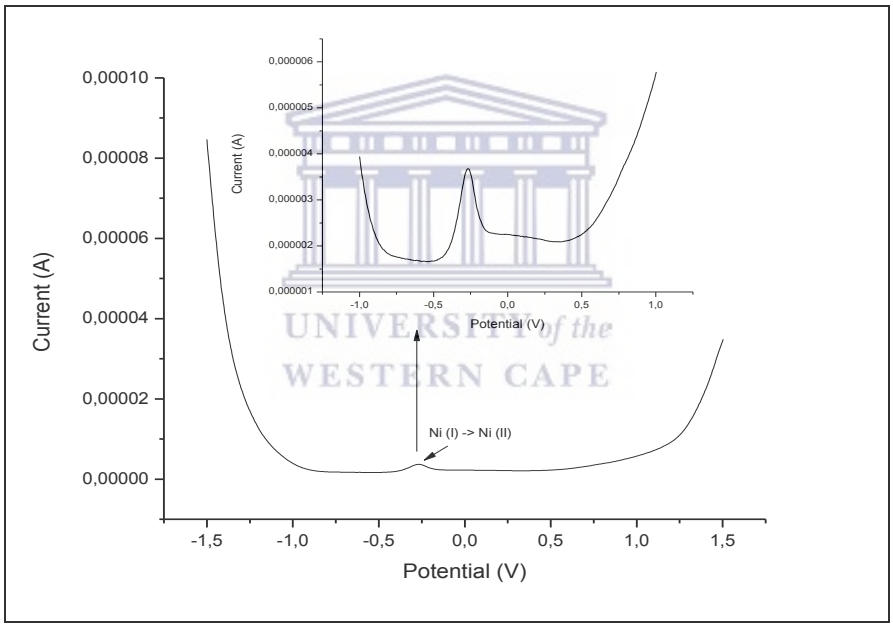

Figure 46: SQW oxidation scan of nickel metal ion (2.5 x 10^{-4} M)

Figure 47 shows the ex-situ approach for the removal of the nickel metal ion. The GCE was modified via the drop-cast method in this approach with the Naf-Sal-DAP modifying ink which was then submerged into the cell containing the nickel metal ions. SQW was applied within the potential range of -1.5 V to 1.8 V for 600 s to allow for complexation

on the electrode surface. The voltammogram proved that complexation had occurred and confirmed by the appearance of the newly observed complex peak at 1.5 V. This peak was shifted to a more positive potential due to of it being harder to oxidize the metal. This was confirmed by the CV of nickel-Sal-DAP complex at bare GCE.

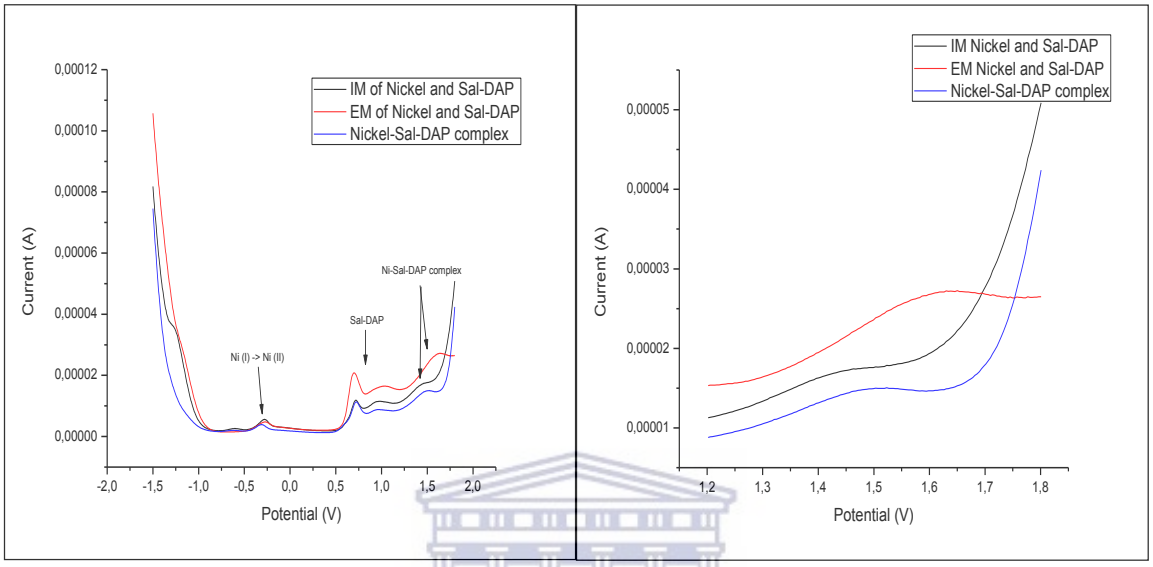

Figure 47: SQW oxidative voltammogram of Ni-Sal-DAP complex@GCE, in-situ and ex-situ methods for Ni-Sal-DAP@GCE

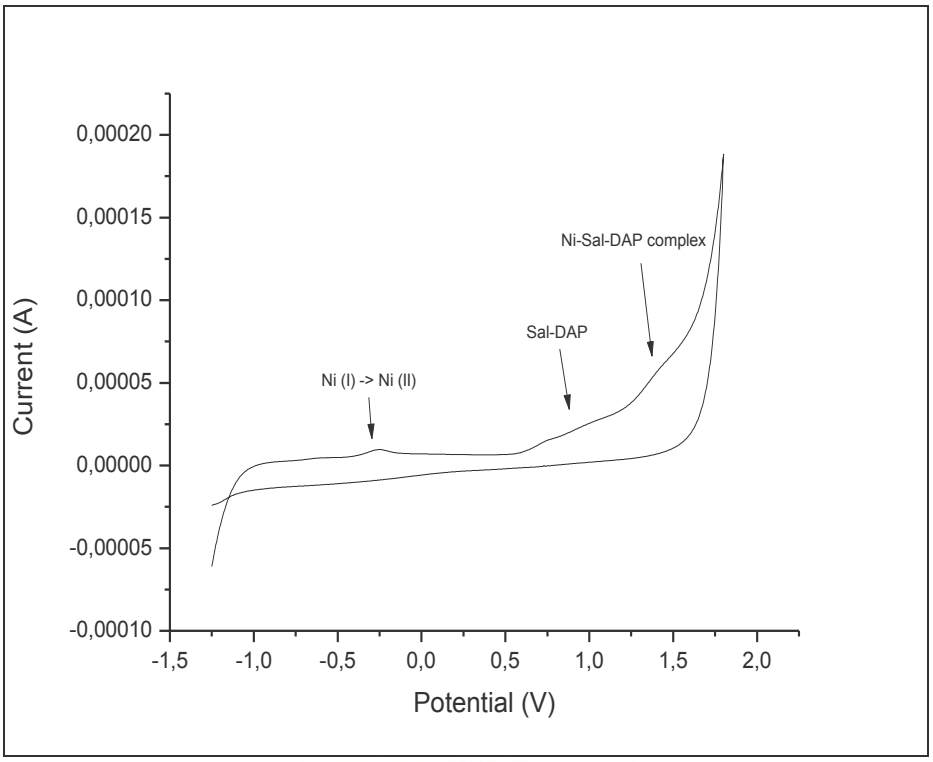

Figure 48: CV of Nickel-Sal-DAP@GCE

SQW of Copper metal ion and Sal-DAP

The cyclic voltammogram (Figure 49) showed the copper peak at a position of -90 mV while the Sal-DAP ligand illustrated a peak at 850 mV with a shoulder at 660 mV. The Cu-Sal-DAP complex, in-situ and ex-situ method experiments were run while taking note of the positions of the copper metal and Sal-DAP peaks.

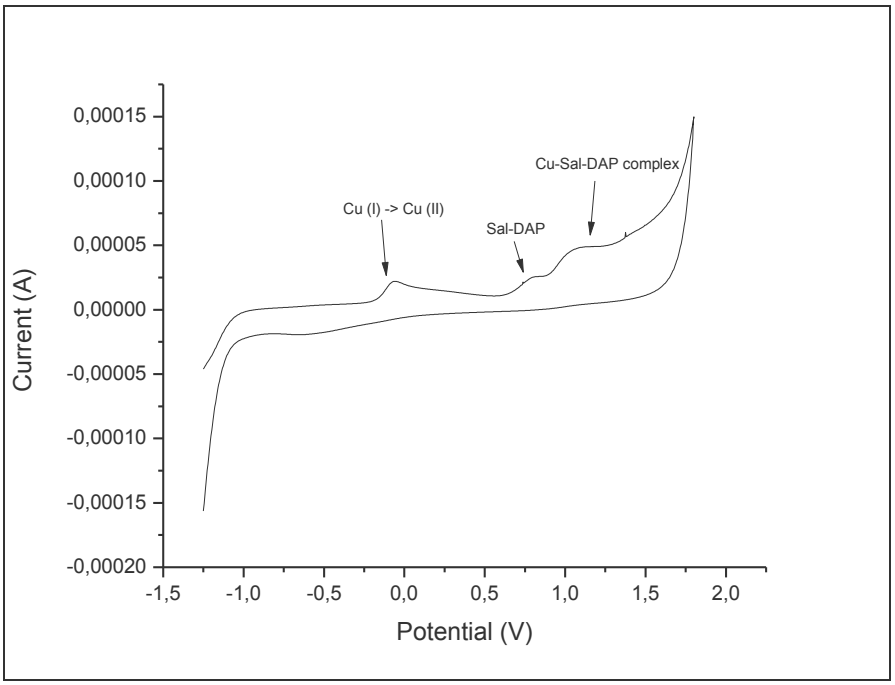

Figure 49: CV of Cu-Sal-DAP complex at bare GCE

For the Cu-Sal-DAP complex, (2.5 x 10^{-4} M) of the complex was added into the EC cell. The SQW voltammetry measurement was done from -1.5 V to 1.8 V and a new peak was detected for the Cu-Sal-DAP complex at a position of 1.0 V (Fig. 50). The new peak is proven to be true by its absence in Figure 50, which is a SQW voltammogram of copper.

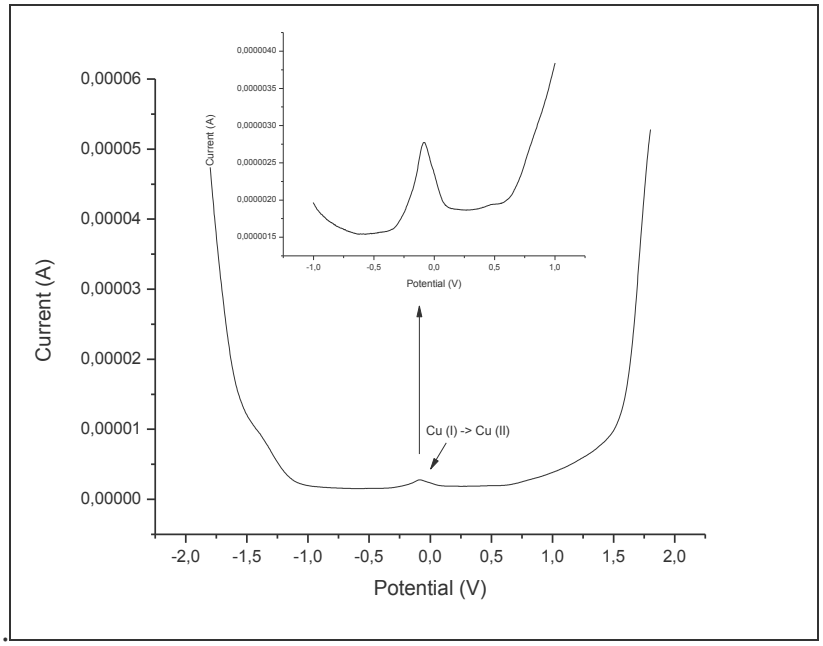

Figure 50: SQW voltammogram copper metal (2.5 x 10^{-4} M) at bare GCE

To run the in-situ mixing method, 2.5 x 10^{-4} M Sal-DAP of ligand and 1 x 10^{-4} M copper metal ion was added to the buffer in the EC cell and allowed to stir. The SQW oxidative scan detected a new peak at 1.1 mV due to complex formation.

Complexation via the ex-situ method consists of coating the GCE with Naf-Sal-DAP@GCE and inserted this into the buffer containing 2.5 x 10^{-5} M copper metal ion.

The SQW scan was run from -1.5 V to 1.8 V at a deposition time of 600s to allow for the complexation at the electrode surface. A new peak was detected for the Cu-Sal-DAP complex at a position of 1.4 V, which was at a more positive potential indicating that it was harder to oxidize the metal. This new peak showed that the ex-situ method was successful for removal of the heavy metal ions by forming the complex at the electrical double layer (Fig. 51).

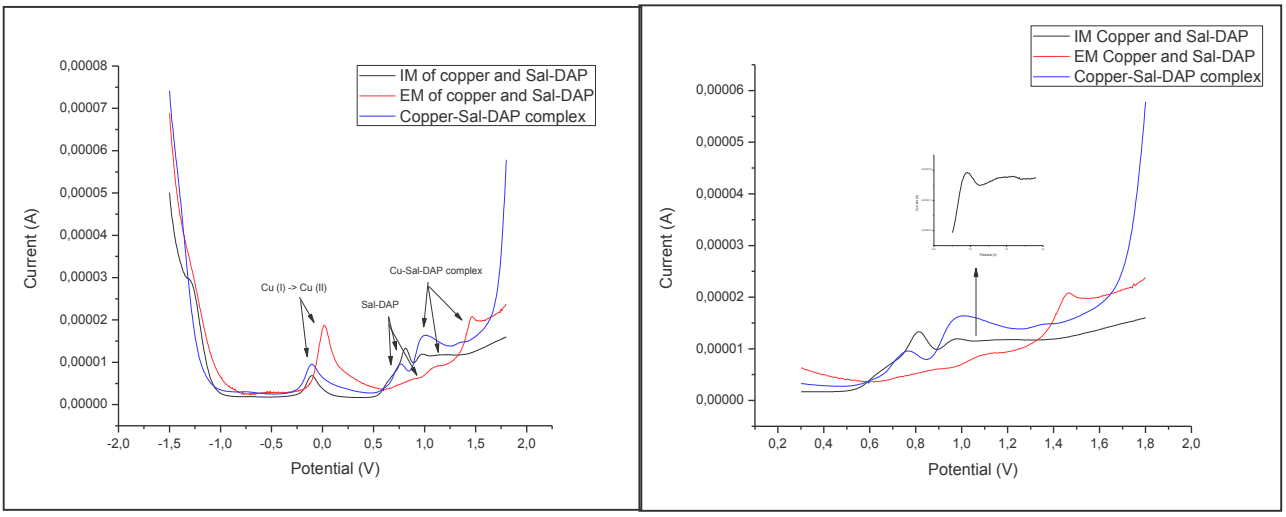

Figure 51: SQW oxidative voltammogram of Cu-Sal-DAP complex at bare GCE, (IM) and (EM)

SQW of Cobalt metal ion and Sal-DAP

SQW and CV voltammograms for cobalt metal and Sal-DAP are shown in Figure 52 and 53 as a basis to investigate whether complexation occurred. The Co-Sal-DAP complex was run first to determine the position of the complex peak.

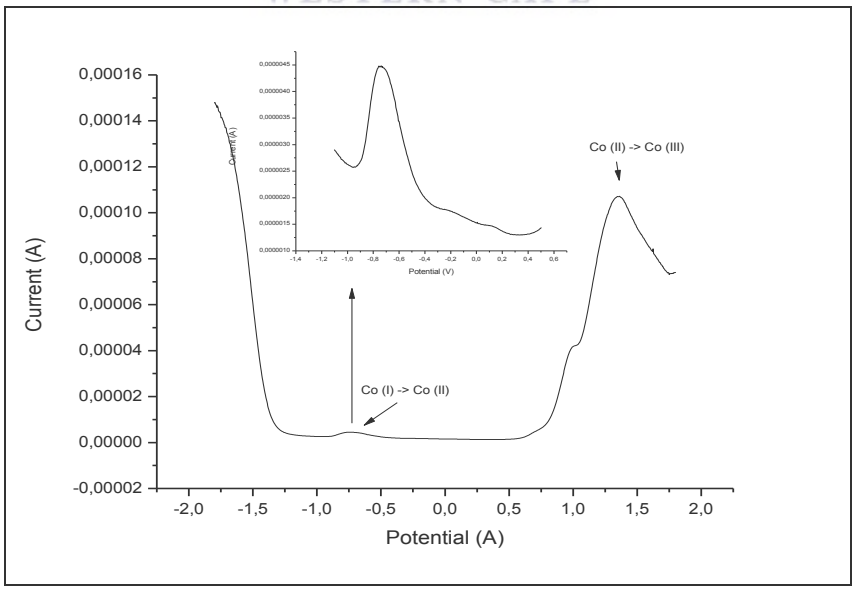

Figure 52: SQW oxidative voltammogram of Co metal ion (2.5 x 10^{-4} M) at bare GCE

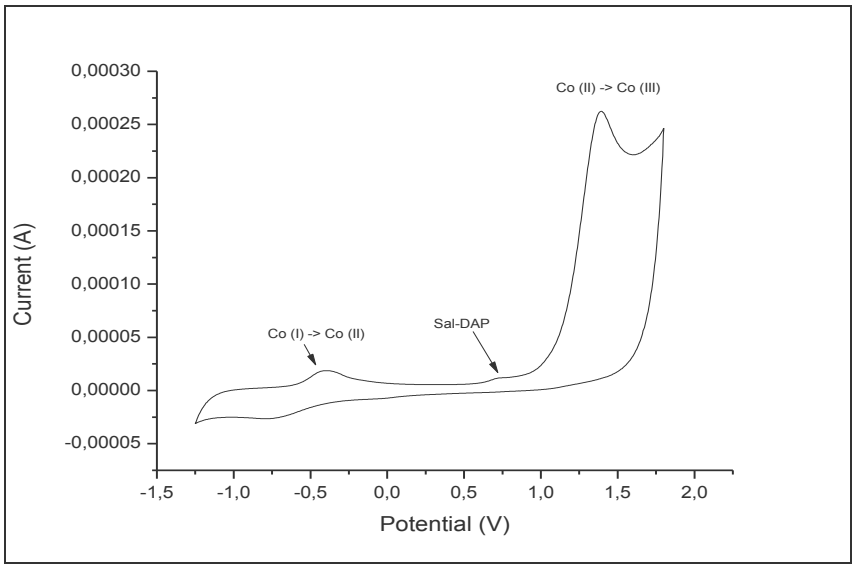

Figure 53: CV of 2.5 x 10^{-4} M Co-Sal-DAP complex at bare GCE

From Figure 54, the peaks for the complex, in-situ mixing, and ex-situ mixing showed no new peak and only the Co and Sal-DAP peaks were observed. This lack of a new peak indicates that the complexation between Sal-DAP was unsuccessful in the PBS buffer via the in-situ and ex-situ method.

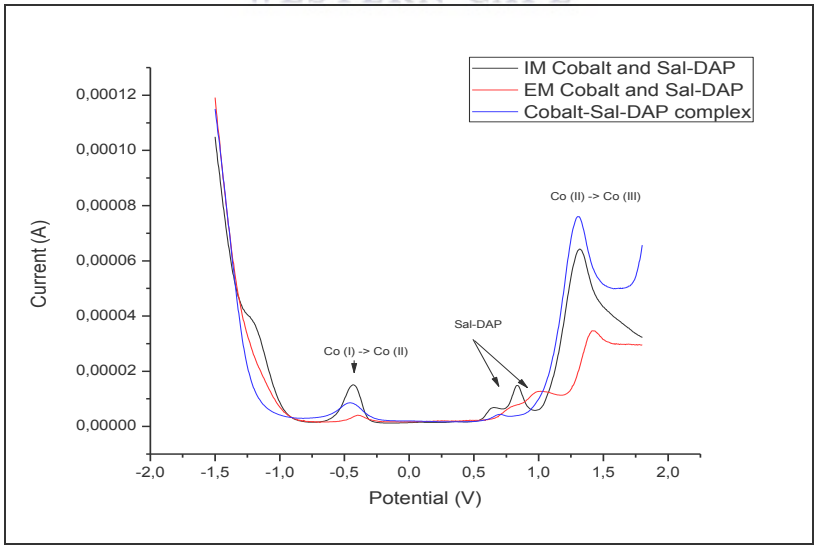

Figure 54: SQW oxidative voltammogram of Co-Sal-DAP complex at bare GCE, in-situ mixing of Co and Sal-DAP ligand and ex-situ mixing Naf-Sal-DAP GCE with Co.

CHAPTER 6: CONCLUSION AND RECOMMENDATIONS

6.1 Conclusion

Heavy metal pollution is one of the most serious environmental problems and thus regulations need to be made more severe.

Many efforts have been developed for different strategies to remove heavy metals from the environment. Electrochemical methods for heavy metal determination provide ways for inexpensive, sensitive and environmentally friendly determination of heavy metals. This work focused on using electrochemical techniques for the simultaneous detection of heavy metal ions such as square-wave anodic stripping voltammetry.

Electrochemical detection of heavy metal ions described in this work was achieved via ligand-metal complexation using Salen-type Schiff base ligands. Two approaches were examined for the complexation of these Schiff base ligands with heavy metal ions, namely in-situ and ex-situ methods. The ex-situ method featured a modification on the glassy carbon electrode (GCE) with Schiff base ligand substrates. The three modified GCE are: Salen coated GCE, reduced graphene oxide-Salen coated GCE and a nafion-Salen coated GCE.

The nafion-Salen coated GCE provided an enhanced sensitive platform suitable for electrochemical extraction. The heavy metals of interest were cobalt, nickel and copper. Two Schiff base ligands viz. Salen and Sal-DAP ligand were used for complexation in which the Salen ligand with Co and Ni ions and Sal- DAP ligand with Cu and Ni metal ions was found to be the best. Results were compared for both approaches in which the ex-situ method demonstrated enhanced electrochemical determination capabilities with

greater sensitivity. This work provided an inexpensive, sensitive and environmentally friendly approach for heavy metal removal.

6.2 Recommendations and future work

Future work related to this study involves the use of alternative, more sensitive and cheaper working electrodes modified with the Schiff base ligands. Since the results of this study proved that modification of electrode surfaces with salen-type ligands shows encouraging proof for electrochemical extraction and determination of heavy metal ions.

Therefore, synthesizing new Schiff base ligands and investigating them for extraction studies should be investigated. In addition, modifying the electrode surface by immobilizing the Schiff base ligand substrates should be explored in order to enhance the removal capacity and detection sensitivity.

BIBLIOGRAPHY

[1] A. Kajal, S. Bala, S. Kamboj, N. Sharma, and V. Saini, "Schiff Bases: A Versatile Pharmacophore," *J. Catal.*, vol. 2013, no. Mic, pp. 1–14, 2013.

[2] A. Abayneh, T. Gebretsadik, S. Tadesse, and M. Thomas, "Synthesis, Spectroscopic, Structural Characterization, Conductivity and Electrochemical Studies of a Schiff Base Ligand and Its Copper Complexes," *Adv. Chem. Eng. Sci.*, vol. 8, pp. 241–254, 2018.

[3] B. Sreenivasulu, *Schiff Base and Reduced Schiff Base Ligands*. 2012.

[4] P. G. Cozzi, C. G. Ciamician, and V. Selmi, "Metal – Salen Schiff base complexes in catalysis: practical aspects," pp. 410–421, 2004.

[5] M. B. R. Bastos, J. C. Moreira, and P. A. M. Farias, "Adsorptive stripping voltammetric behaviour of UO2 (II) complexed with the Schiff base N,N-ethylenebis (salicylidenimine) in aqueous 4-(2-hydroxyethyl)-1-piperazine ethanesulfonic acid medium," *Anal. Chim. Acta*, vol. 408, pp. 83–88, 2000.

[6] F. Sunday Nworie, "Bis(Salicylidene)Ethylenediamine(Salen) and Bis(Salicylidene)Ethylenediamine-Metal Complexes: from Structure to Biological Activity," *J. Anal. Pharm. Res.*, vol. 3, no. 6, pp. 1–10, 2016.

[7] N. Nuñez-dallos, C. Cuadrado, J. Hurtado, E. Nagles, and O. García-beltran, "In situ-Mercury Film Electrode for Simultaneous Determination of Lead and Cadmium Using Nafion Coated New Coumarin Schiff Base as Chelating-Adsorbent," *Int. J. Electrochem. Sci.*, vol. 11, pp. 9855–9867, 2016.

[8] G. Crisponi, L. Sibous, E. Bentouhami, and M. A. Khan, "Synthesis, Characterization, and Electrochemical Behaviour of Cobalt (II) and Nickel (II) Complexes with N2O2 Chelating Ligand 4,4 '-(Biphenyl-4,4'-diyldinitrilo)-dipentan-2-one," *J. Inorg. Chem.*, 104979, 2013.

[9] P. Augusto, M. Farias, M. Bethlem, and R. Bastos, "Electrochemical Behavior of Ni (II)-Salen at the Mercury Electrode," *Int. J. Electrochem.*, 257926, 2013.

[10] D. Çakmak, S. Çakran, S. Yalçinkaya, and C. Demetgül, "Synthesis of salen-type Schiff base metal complexes, electropolymerization on graphite electrode surface and investigation of electrocatalytic effects," *J. Electroanal. Chem.*, vol. 808, pp. 65–74, 2018.

[11] V. B. Badwaik, R. D. Deshmukh, and A. S. Aswar, "Transition metal complexes of a Schiff base: Synthesis, characterization, and antibacterial studies," *J. Coord. Chem.*, vol. 62, no. 12, pp. 2037–2047, 2009.

[12] V. Masindi and K. L. Muedi, "Environmental Contamination by Heavy Metals," in *Heavy Metals*, 2018, pp. 115–133.

[13] R. K. Gautam, S. K. Sharma, S. Mahiya, and M. C. Chattopadhyaya, "CHAPTER 1. Contamination of Heavy Metals in Aquatic Media: Transport, Toxicity and Technologies for Remediation," *Heavy Met. Water*, no. October, pp. 1–24, 2014.

[14] S. MEK and S. AM, "Heavy Metals Contaminants in Water and Fish from Four

Different Sources in Sudan," *J. Infect. Dis. Ther.*, vol. 04, no. 02, pp. 2–5, 2016.

[15] M. Lambert, B. Leven, and R. M. Green, "New Methods of Cleaning Up Heavy Metal in Soils and Water," *Environ. Sci. Technol. Briefs Citizens*, pp. 1–3, 2000.

[16] P. B. Tchounwou, C. G. Yedjou, A. K. Patlolla, and D. J. Sutton, "Heavy Metal Toxicity and the Environment," in *Molecular, Clinical and Environmental Toxicology*, 2012, pp. 133–164.

[17] M. Jaishankar, T. Tseten, N. Anbalagan, B. B. Mathew, and K. N. Beeregowda, "Toxicity, mechanism and health effects of some heavy metals," *Interdiscip. Toxicol.*, vol. 7, no. 2, pp. 60–72, 2014.

[18] P. Lentini, L. Zanoli, A. Granata, S. S. Signorelli, P. Castellino, and R. Dell'Aquila, "Kidney and heavy metals - The role of environmental exposure (Review)," *Mol. Med. Rep.*, vol. 15, no. 5, pp. 3413–3419, 2017.

[19] B. E. Igiri, S. I. R. Okoduwa, G. O. Idoko, E. P. Akabuogu, A. O. Adeyi, and I. K. Ejiogu, "Toxicity and Bioremediation of Heavy Metals Contaminated Ecosystem from Tannery Wastewater: A Review," *J. Toxicol.*, vol. 2018, pp. 1–16, 2018.

[20] M. S. Sankhla, M. Kumari, M. Nandan, R. Kumar, and P. Agrawal, "Heavy Metals Contamination in Water and their Hazardous Effect on Human Health-A Review," *Int. J. Curr. Microbiol. Appl. Sci.*, vol. 5, no. 10, pp. 759–766, 2016.

[21] K. Pokpas, "Graphene-Modified Pencil Graphite Bismuth- Film Electrodes for the Determination of Heavy Metals in Water Samples Using Anodic Stripping Voltammetry," University of the Western Cape, 2013.

[22] A. Mohadesi, E. Teimoori, M. A. Taher, and H. Beitollah, "Adsorptive stripping voltammetric determination of cobalt (II) on the carbon paste electrode," *Int. J. Electrochem. Sci.*, vol. 6, no. 2, pp. 301–308, 2011.

[23] P. Augusto, M. Farias, M. Bethlem, and R. Bastos, "Electrochemical Behavior of Copper(II) salen in Aqueous Phosphate Buffer at the Mercury Electrode," vol. 4, pp. 458–470, 2009.

[24] Y. Shimazaki, "Oxidation Chemistry of Metal (II) Salen-Type Complexes," IntechOpen, UK, 2013.

[25] C. Xiang, Y. Zou, J. Xie, X. Fei, and J. Li, "Nafion-modified glassy carbon electrode for trace determination of indium," *Anal. Lett.*, vol. 38, no. 13, pp. 2045–2055, 2005.

[26] A. Leniart, M. Brycht, B. Burnat, and S. Skrzypek, "An application of a glassy carbon electrode and a glassy carbon electrode modified with multi-walled carbon nanotubes in electroanalytical determination of oxycarboxin," *Ionics (Kiel).*, vol. 24, no. 7, pp. 2111–2121, 2018.

[27] I. G. David, D. E. Popa, M. Buleandra, Z. Moldovan, E. E. Iorgulescu, and I. A. Badea, "Cheap pencil graphite electrodes for rapid voltammetric determination of chlorogenic acid in dietary supplements," *Anal. Methods*, vol. 8, no. 35, pp. 6537–6544, 2016.

[28] S. Azhari, P. Sathishkumar, R. Ahamad, F. Ahmad, and A. R. M. Yusoff, *Fabrication of a composite modified glassy carbon electrode: A highly selective, sensitive and rapid electrochemical sensor for silver ion detection in river water samples*, vol. 8, no. 28. 2016.

[29] P. Chooto, "Modified Electrodes for Determining Trace Metal Ions."

[30] M. Baalousha, W. How, E. Valsami-Jones, and J. R. Lead, *Overview of Environmental Nanoscience*, 1st ed., vol. 7. Elsevier Ltd., 2014.

[31] S. Luby, M. Lubyova, P. Siffalovi, M. Jergel, E. Majkova, *A Brief History of Nanoscience and Foresight in Nanotechnology, A Complex Review of Current Hot Topics and their Applications*, in Nanomaterials and Nanoarchitectures Eds M. Bardosova, T. Wagne Eds, Springer Netherlands 2015.

[32] J. E. Hulla, S. C. Sahu, and A. W. Hayes, "Nanotechnology: History and future," *Hum. Exp. Toxicol.*, vol. 34, no. 12, pp. 1318–1321, 2015.

[33] A Dowling, R Clift, N Grobert *et al.*, "Nanoscience and nanotechnologies: opportunities and uncertainties," *London R. Soc. R. Acad. Eng. Rep.*, vol. 46, no. July, pp. 618–618, 2004.

[34] V. Uskoković, "Entering the era of nanoscience: Time to be so small," *J. Biomed. Nanotechnol.*, vol. 9, no. 9, pp. 1441–1470, 2013.

[35] J. Behari, "Principles of nanoscience: An overview," *Indian J. Exp. Biol.*, vol. 48, no. 10, pp. 1008–1019, 2010.

[36] S. Kumar, N. and Khumbat, "Unique properties 8.1," in *Essentials in Nanoscience and Nanotechnology, First Edition*, 2016, pp. 326–360.

[37] M. F. Hochella *et al.*, "Natural, incidental, and engineered nanomaterials and their impacts on the Earth system," *Science* vol. 363, no. 6434, 2019.

[38] M. G. M. Krystek, "Nanomaterials in structural engineering," in *IntechOpen*, 2018, pp. 115–131.

[39] D. A. C. Brownson, G. C. Smith, and C. E. Banks, "Graphene oxide electrochemistry: The electrochemistry of graphene oxide modified electrodes reveals coverage dependent beneficial electrocatalysis," *R. Soc. Open Sci.*, vol. 4, no. 11, 2017.

[40] E. P. Randviir, D. A. C. Brownson, and C. E. Banks, "A decade of graphene research: Production, applications and outlook," *Mater. Today*, vol. 17, no. 9, pp. 426–432, 2014.

[41] A. Pareek, J. Shanthi Sravan, and S. Venkata Mohan, "Graphene modified electrodes for bioelectricity generation in mediator-less microbial fuel cell," *J. Mater. Sci.*, vol. 54, no. 17, pp. 11604–11617, 2019.

[42] Q. Yan, J. Li, X. Zhang, J. Zhang, and Z. Cai, "Mass production of graphene materials from solid carbon sources using a molecular cracking and welding method," *J. Mater. Chem. A*, vol. 7, no. 23, pp. 13978–13985, 2019.

[43] F. Yu, C. Wang, and J. Ma, "Applications of graphene-modified electrodes in microbial fuel cells," *Materials (Basel).*, vol. 9, no. 10, 2016.

[44] A. T. Smith, A. M. LaChance, S. Zeng, B. Liu, and L. Sun, "Synthesis, properties, and applications of graphene oxide/reduced graphene oxide and their nanocomposites," *Nano Mater. Sci.*, vol. 1, no. 1, pp. 31–47, 2019.

[45] S. S. Shams, R. Zhang, and J. Zhu, "Graphene synthesis: A Review," *Mater. Sci. Pol.*, vol. 33, no. 3, pp. 566–578, 2015.

[46] H. C. Lee *et al.*, "Review of the synthesis, transfer, characterization and growth mechanisms of single and multilayer graphene," *RSC Adv.*, vol. 7, no. 26, pp. 15644–15693, 2017.

[47] N. Lozano *et al.*, "A blueprint for the synthesis and characterisation of thin graphene oxide with controlled lateral dimensions for biomedicine," *2D Mater.*, vol. 5, no. 3, p. 035020, 2018.

[48] et al. Md. Sajibul Alam Bhuyan, "Synthesis of graphene," *Int. Nano Lett*, vol. 6, pp. 65–83, 2016.

[49] A. Dato, "Graphene synthesized in atmospheric plasmas - A review," *J. Mater. Res.*, vol. 34, no. 1, pp. 214–230, 2019.

[50] K. V. and G. P. D. C. Wang, "Large-Area Synthesis and Growth Mechanism of Graphene by Chemical Vapor Deposition," *IntechOpen*, vol. 5, pp. 97–113, 2018.

[51] X. J. Lee *et al.*, "Review on graphene and its derivatives: Synthesis methods and potential industrial implementation," *J. Taiwan Inst. Chem. Eng.*, vol. 98, pp. 163–180, 2019.

[52] S. N. Alam, N. Sharma, and L. Kumar, "Synthesis of Graphene Oxide (GO) by Modified Hummers Method and Its Thermal Reduction to Obtain Reduced Graphene Oxide (rGO)*," *Graphene*, vol. 06, no. 01, pp. 1–18, 2017.

[53] Z. Wang, "Progress on preparation of graphene and its application," *IOP Conf. Ser. Mater. Sci. Eng.*, vol. 242, no. 1, 2017.

[54] S. Sali, H. R. Mackey, and A. A. Abdala, "Effect of Graphene Oxide Synthesis Method on Properties and Performance of Polysulfone-Graphene Oxide Mixed Matrix Membranes," *Nanomaterials*, vol. 9, no. 5, p. 769, 2019.

[55] A. Allahresani, "Mn (III) salen complex supported on graphene oxide nanosheets as a highly selective and recoverable catalyst for the oxidation of sulfides," vol. 6, pp. 180–191, 2018.

[56] A. Saroja and B. R. Bhat, "Cobalt Schiff Base Immobilized on a Graphene Nanosheet with," *Ind. Eng. Chem. Res.*, vol. 58, pp. 590–601, 2018.

[57] X. Makhoba and A. Pouris, "Bibliometric analysis of the development of nanoscience research in South Africa," *S. Afr. J. Sci.*, vol. 113, no. 11–12, pp. 1–9, 2017.

[58] M. F. Khanfar *et al.*, "Ag/Au modified nafion coated glassy carbon electrode for the detection of metronidazole," *Int. J. Electrochem. Sci.*, vol. 14, no. 4, pp. 3265–3280, 2019.

[59] R. F. Vreeland *et al.*, "Biocompatible PEDOT:Nafion composite electrode coatings for selective detection of neurotransmitters in vivo," *Anal. Chem.*, vol.

87, no. 5, pp. 2600–2607, 2015.

[60] N. A. Papadopoulou, A. B. Florou, and M. I. Prodromidis, "Sensitive determination of iron using disposable Nafion-Coated Screen-Printed graphite electrodes," *Anal. Lett.*, vol. 51, no. 1–2, pp. 198–208, 2018.

[61] T. K. Tran, H. J. Leu, K. F. Chiu, and C. Y. Lin, "Electrochemical Treatment of Heavy Metal-containing Wastewater with the Removal of COD and Heavy Metal Ions," *J. Chinese Chem. Soc.*, vol. 64, no. 5, pp. 493–502, 2017.

[62] A. E. Segneanu *et al.*, *Waste water tretment methods*. 2013.

[63] D. Zamboulis, E. N. Peleka, N. K. Lazaridis, and K. A. Matis, "Metal ion separation and recovery from environmental sources using various flotation and sorption techniques," *J. Chem. Technol. Biotechnol.*, vol. 86, no. 3, pp. 335–344, 2011.

[64] G. A. Tonini and L. A. M. Ruotolo, "Heavy metal removal from simulated wastewater using electrochemical technology: optimization of copper electrodeposition in a membraneless fluidized bed electrode," *Clean Technol. Environ. Policy*, vol. 19, no. 2, pp. 403–415, 2017.

[65] S. K. Gunatilake, "Methods of Removing Heavy Metals from Industrial Wastewater," *J. Multidiscip. Eng. Sci. Stud.*, vol. 1, no. 1, pp. 12–18, 2015.

[66] C. Zhang, B. Chen, Y. Bai, and J. Xie, "A new functionalized reduced graphene oxide adsorbent for removing heavy metal ions in water via coordination and ion exchange," *Sep. Sci. Technol.*, vol. 53, pp. 2896-2905, 2018.

[67] A. Azimi, A. Azari, M. Rezakazemi, and M. Ansarpour, "Removal of Heavy Metals from Industrial Wastewaters: A Review," *ChemBioEng Rev.*, vol. 4, no. 1, pp. 37–59, 2017.

[68] T. K. Tran, K. F. Chiu, C. Y. Lin, and H. J. Leu, "Electrochemical treatment of wastewater: Selectivity of the heavy metals removal process," *Int. J. Hydrogen Energy*, vol. 42, no. 45, pp. 27741–27748, 2017.

[69] W. Mihoubi, E. Sahli, A. Gargouri, and C. Amiel, "FTIR spectroscopy of whole cells for the monitoring of yeast apoptosis mediated by p53 over-expression and its suppression by Nigella sativa extracts," *PLoS One*, vol. 12, no. 7, pp. 1–16, 2017.

[70] B. Hofko *et al.*, "FTIR spectral analysis of bituminous binders: reproducibility and impact of ageing temperature," *Mater. Struct. Constr.*, vol. 51, no. 2, 2018.

[71] M. J. Baker, E. Gazi, M. D. Brown, J. H. Shanks, P. Gardner, and N. W. Clarke, "FTIR-based spectroscopic analysis in the identification of clinically aggressive prostate cancer," *Br. J. Cancer*, vol. 99, no. 11, pp. 1859–1866, 2008.

[72] Y. S. Leong *et al.*, "UV-vis spectroscopy: A new approach for assessing the color index of transformer insulating oil," *Sensors (Switzerland)*, vol. 18, no. 7, pp. 1–15, 2018.

[73] E. Tomaszewska *et al.*, "Detection Limits of DLS and UV-Vis Spectroscopy in Characterization of Polydisperse Nanoparticles Colloids" *J. Nanomater.*, 313081,

2013.

[74] L. D. Yadav, "Ultraviolet and Visible Spectroscopy," in *Organic Spectroscopy*, 2005, pp. 7–51.

[75] Z. Y., Z. H., C. D., G. F., P. H., and Y. Y., "Metabolomics approach by 1H NMR spectroscopy of serum reveals progression axes for asymptomatic hyperuricemia and gout," *Arthritis Res. Ther.*, vol. 20, no. 1, pp. 1–11, 2018.

[76] E. Hatzakis, "Nuclear Magnetic Resonance (NMR) Spectroscopy in Food Science: A Comprehensive Review," *Compr. Rev. Food Sci. Food Saf.*, vol. 18, no. 1, pp. 189–220, 2019.

[77] V. H. Pomin, "Unravelling Glycobiology by NMR Spectroscopy," in *Intech*, 2012, pp. 63–98.

[78] L. D. S. Yadav, "C NMR Spectroscopy 6.1," in *Organic Spectroscopy*, 2005, pp. 195–223.

[79] Y. Yang *et al.*, "Evaluating different extraction solvents for GC-MS based metabolomic analysis of the fecal metabolome of adult and baby giant pandas," *Sci. Rep.*, vol. 9, no. 1, pp. 1–9, 2019.

[80] C. Shackleton, O. J. Pozo, and J. Marcos, "GC/MS in Recent Years Has Defined the Normal and Clinically Disordered Steroidome: Will It Soon Be Surpassed by LC/Tandem MS in This Role?" *J. Endocr. Soc.*, vol. 2, no. 8, pp. 974–996, 2018.

[81] N. Elgrishi, K. J. Rountree, B. D. McCarthy, E. S. Rountree, T. T. Eisenhart, and J. L. Dempsey, "A Practical Beginner's Guide to Cyclic Voltammetry," *J. Chem. Educ.*, vol. 95, no. 2, pp. 197–206, 2018.

[82] W. R. A. H. Weppner, "Electrochemical methods for determining antibiotics," *Pharmazie*, vol. 29, no. 12, pp. 752–756, 1974.

[83] S. H. Jordanov, "The third century of electrochemistry: Lowering the horizon or raising it further?" *J. Serbian Chem. Soc.*, vol. 78, no. 12, pp. 2165–2177, 2013.

[84] P. Monk, *Fundamentals of Electro-Analytical Chemistry*, *Wiley*, 2001.

[85] S. Mendoza, E. Bustos, J. Manríquez, and L. A. Godínez, "Voltammetric Techniques," *Agric. Food Electroanal.*, pp. 21–48, 2015.

[86] F. Scholz, *Electroanalytical Methods*. Springer, 2005.

[87] B. Uslu, "The Analytical Applications of Square Wave Voltammetry on Pharmaceutical Analysis," *Open Chem. Biomed. Methods J.*, vol. 3, no. 1, pp. 56–73, 2011.

[88] A. J. Bard, L. R. Faulkner, E. Swain, and C. Robey, *Electrochemical Methods: Fundamentals and Applications*, Wiley, 2000.

[89] O. Fischer and E. Fischerová, "Basic principles of voltammetry," *Exp. Tech. Bioelectrochemistry*, pp. 41–157, 1995.

[90] P. K. M. K. Mahato, S. Kumar, A. Srivastava, *Electrochemical Immunosensors*. Elsevier Inc., 2018.

[91] D. Adrienko, "Electrochemistry Fundamentals," in *Cyclic Voltammetry*, 2008, p. 12.

[92] M. R. L. Khalafi, "Cyclic Voltammetry," *Encyclopedia of Physical Organic Chemistry*, no. First Edition. 2017.

[93] M. Lovric, "Square-Wave Voltammetry," in *Electroanalytical methods*, 2005, pp. 113–136.

[94] V. Mirceski, R. Gulaboski, M. Lovric, I. Bogeski, R. Kappl, and M. Hoth, "Square-Wave Voltammetry: A Review on the Recent Progress," *Electroanalysis*, vol. 25, no. 11, pp. 2411–2422, 2013.

[95] L. S. V. Mirceski, S. Skrzypek and L Stojanov "Square-wave voltammetry" ChemTexts., vol. 4, p. 1-17, 2018.

[96] K. Jeremiah Aoki and J. Chen, "Tips of Voltammetry," *Voltammetry*, pp. 1–19, 2019.

[97] A. L. Laina, "Voltammetric sensors for the determination of pharmaceuticals," Cochin University of Science and Technology, 2013.

[98] N. I. Zaaba, K. L. Foo, U. Hashim, S. J. Tan, W. W. Liu, and C. H. Voon, "Synthesis of Graphene Oxide using Modified Hummers Method: Solvent Influence," *Procedia Eng.*, vol. 184, pp. 469–477, 2017.

[99] K. Naseem *et al.*, "Extraction of Heavy Metals from Aqueous Medium by Husk Biomass: Adsorption Isotherm, Kinetic and Thermodynamic study," *Zeitschrift fur Phys. Chemie*, vol. 233, no. 2, pp. 201–223, 2019.